Dynamics of a horizontal thin liquid film in the presence of reactive surfactants

A. Pereira and P. M. J. Trevelyan[a)]
Department of Chemical Engineering, Imperial College London, London SW7 2AZ, United Kingdom

U. Thiele[b)]
Max-Planck-Institut für Physik komplexer Systeme, Nöthnitzer Str. 38, D-01187 Dresden, Germany

S. Kalliadasis
Department of Chemical Engineering, Imperial College London, London SW7 2AZ, United Kingdom

(Received 14 February 2007; accepted 23 July 2007; published online 9 November 2007)

We investigate the interplay between a stable horizontal thin liquid film on a solid substrate and an excitable or bistable reactive mixture on its free surface. Their coupling is twofold. On the one hand, flow in the film transports the reacting surfactants convectively. On the other hand, gradients in the surfactant concentration exert Marangoni stresses on the free surface of the film. A reduced model is derived based on the long-wave approximation. We analyze the linear stability of the coupled system as well as the nonlinear behavior, including the propagation of solitary waves, fronts, and pulses. We show, for instance, that the coupling of thin film hydrodynamics and surfactant chemistry can either stabilize instabilities occurring in the pure chemical system, or in a regime where the pure hydrodynamic and chemical subsystems are both stable, the coupling can induce instabilities. © *2007 American Institute of Physics*. [DOI: 10.1063/1.2775938]

I. INTRODUCTION

A thin liquid film on a solid substrate, either bounded, e.g., a droplet, or unbounded, has over the years proven to be an important prototype at the core of many industrial processes and applications, such as lubrication and coating, as well as biological problems for which it is necessary to understand and control flows at a small scale.[1,2] Numerous studies have thus been devoted to the statics and dynamics of thin films in different settings and configurations and in particular of simple liquids in isothermal conditions: film rupture and coarsening,[3–6] falling films,[7–10] fingering instabilities of advancing film fronts,[11–14] film and droplet evaporation,[15–17] and sliding or rolling droplets.[18,19]

As an example, falling liquid films have received considerable attention for several decades since the pioneering study by Kapitza.[20] The primary instability of the flat film base flow is driven by the classical long-wave mode first observed in the experiments by Kapitza and Kapitza.[21] After the instability onset, the primary wave field undergoes a sequence of wave transitions and is eventually transformed into a train of solitary pulses (see Ref. 22 for a detailed analysis of the wave transitions). We note that Benney[23] was the first to apply, for the falling problem, a long-wave expansion leading to a single equation of the evolution type for the free surface. Subsequently, the so-called "long-wave approximation" introduced by Benney has been central to many other thin film studies (see, e.g., Refs. 1 and 2).

Another example that has received considerable attention over the years is the dynamics of droplets on a substrate. In addition to the presence of a free boundary, we now encounter several other challenging aspects and complexities including the presence of a moving contact line and the associated singularity at the three-phase conjunction as well as the wettability characteristics of the substrate which play a crucial role in the liquid-solid interaction.[24–26]

The dynamics of thin films is often influenced by concentration/temperature dependent fluid physical properties, in particular surface tension gradients due to the thermal Marangoni effect associated with spatially inhomogeneous temperature fields and the solutal Marangoni effect associated with the presence of surface active substances, i.e., surfactants. The role of the thermal Marangoni effect in generating fluid motion was established by Pearson[27] and Sternling and Scriven.[28] Pearson discovered a short-wave mode that does not require a deformable free surface and is responsible for the formation of convection rolls in the Bénard experiment with a horizontal temperature gradient. Sternling and Scriven, on the other hand, obtained a long-wave mode that leads to deformation of the interface. The role of the two modes in the instability onset for the problem of a film falling down a uniformly heated plane was scrutinized by Goussis and Kelly.[29] Recent work on this problem has focused on the nonlinear wave regime.[30–33]

The role of the solutal Marangoni effect in generating fluid motion was first examined by Sternling and Scriven[34] for a two-phase system with soluble surfactants. They demonstrated that a stationary instability arises whenever the surfactant is transferred out of the phase in which its diffusivity is lower, while the system is always stable when the transfer is in the opposite direction. Oscillatory instability can also appear for transfer in any direction when the kinematic vis-

[a)]Present address: Centre for Nonlinear Phenomena and Complex Systems, CP 231, Université Libre de Bruxelles, 1050 Brussels, Belgium.
[b)]Present address: School of Mathematics, Loughborough University, Loughborough LE11 3TU, United Kingdom.

cosity and the surfactant diffusivity are both lower in one phase. The influence of soluble surfactants on the linear instability of falling films has been investigated by Ji and Setterwall[35] and Shkadov *et al.*[36] On the other hand, insoluble surfactants always have a stabilizing influence as was demonstrated in the early study by Ruckenstein and Jain for a thin film in the presence of insoluble surfactants[37] (see also Jensen and Grotberg[38]). Indeed, to obtain an instability with insoluble surfactants on the surface of the film one requires a source of surfactants. The resulting instability typically leads to rupture of the film (see, e.g., Matar[39]). A detailed analysis of the spreading dynamics of insoluble surfactants on thin films, including shock evolution and rupture is given by Jensen and Grotberg.[38]

It is then clear that thin liquid films often exhibit a very rich pattern formation dynamics. Another class of well-studied problems that also shows a rich pattern forming behavior is that of reaction-diffusion systems, often encountered in the fields of chemistry and biology. In contrast to the above hydrodynamic systems where the patterns result from the action of a driving force on the flow, such as gravity (as in the falling films case) or thermal/solutal Marangoni effects, in reaction-diffusion systems the patterns typically result from the competition between diffusion and nonlinear reactions which frequently involve autocatalytic steps. Well studied examples in the absence of diffusion are the celebrated Belousov-Zhabotinsky reaction,[40–43] its Oregonator reduction,[44] the Brusselator model,[45] and the Gray-Scott model.[46] These systems are spatially homogenous but they can exhibit complex temporal behavior including transition to chaos, unlike, e.g., the Bénard experiment mentioned earlier which displays spatial inhomogeneity.

One of the most widely studied reaction-diffusion system is the FitzHugh-Nagumo system, a relatively simple prototype that arose originally in the biological field as a model for the axon of a nerve cell.[47] It is of paradigmatic value, not only because it is a comparatively simple prototype for complex spatio-temporal behavior resulting from the coupling between chemical reactions and diffusion, but also because it is well understood and has been applied to many different physical settings.[48–51] The destabilization of the base state for this system quite frequently results in the formation of spatially periodic steady states (so called "Turing patterns") or in an oscillatory behavior in time as well as in a wide variety of wave patterns. These patterns are strongly linked to the two regimes which typically characterize the FitzHugh-Nagumo system: depending on the values of the parameters describing the reaction, we can have *bistability* or *excitability*. A bistable system possesses two stable uniform steady states and *fronts* connecting the two are likely to propagate in it. For an excitable system on the other hand, a small but finite perturbation can drive the system far from its initial uniform steady state. This property often leads to the propagation of *pulses*. In two dimensions more complicated patterns such as spiral or scroll waves can be observed.

Hydrodynamic and reaction-diffusion systems are seemingly unrelated and are mostly studied separately. However, in many important cases the combined effect of convection on chemical reactions and the influence of Marangoni stresses on the dynamics of a fluid interface, come to the fore and cannot always be neglected. This interdependence can even result in new pattern forming behavior. The coupling between the chemistry and the hydrodynamics in this context can be achieved by including dependencies of the bulk viscosity and density of reactant concentration as was done in Hele-Shaw flows[52–56] or through the thermal Marangoni effect induced by exothermic chemical reactions as was done in falling liquid films.[57–59]

Another possibility is to couple the hydrodynamics with the reaction-diffusion process through a surface active agent involved in the chemical reaction. A reactive surfactant might act at the liquid/substrate or at the liquid/gas interface. In the first case, for example, Dos Santos and Ondarçuhu[60] have taken advantage of the ability of *n*-alkane molecules to alter the wettability of glass or silicon to show that a chemical reaction taking place at the substrate can cause a droplet to run. Other examples of driven droplets have been reported by Lee *et al.*[61] and Sumino *et al.*.[62] Theoretical descriptions include estimations for droplet velocities based on force equilibria,[63] but also dynamical models based on (long-wave) thin film equations.[64,65]

In the present study, we examine the interaction between the free-surface dynamics of a horizontal thin film and reactive surfactants at the liquid/air interface. Related studies are sparse in the literature. Noted exceptions are the works by Pismen[66] and Dagan and Pismen[67] that examined the interaction between propagating chemical fronts and thin film hydrodynamics. The first study considered a single autocatalytic reaction on a nondeformable surface involving a soluble surfactant supplied to the surface from the bulk. In this case, the coupling between chemistry and hydrodynamics can lead to some complex flow patterns in the bulk. The second study allowed the interface to deform while the surfactant was assumed to be insoluble. The chemical scheme, a single multistable chemical reaction maintaining two different steady concentration states at the far ends of the film, can lead to a propagating chemical wave on the surface. In another study undertaken by Buyevich *et al.*[68] the chemical reaction takes place at the interface between two liquids.

Here, we adopt a chemical system that exhibits a much richer behavior than the above settings. More specifically, we employ the earlier introduced FitzHugh-Nagumo system to model a reactive mixture of two surface active species one of which acts as a strong surfactant. This is a system of two equations for the evolution in time and space of two variables, frequently referred to as the *activator* and *inhibitor*. As discussed earlier this prototype represents a simple model for a two species chemical system showing both excitable and bistable regimes. Here both reactants are transported convectively through the film flow and also diffuse along the surface. For simplicity we assume that the film is driven by the surface-active properties of the inhibitor. On the other hand the activator is only weakly surface active. Hence, both film and inhibitor have typical wavelengths of the same order. Assuming that this wavelength is long compared to the undisturbed film thickness, so that both film and inhibitor are "long-wave" variables, allows us to perform a long-wave approximation of the full system resulting in a set of three

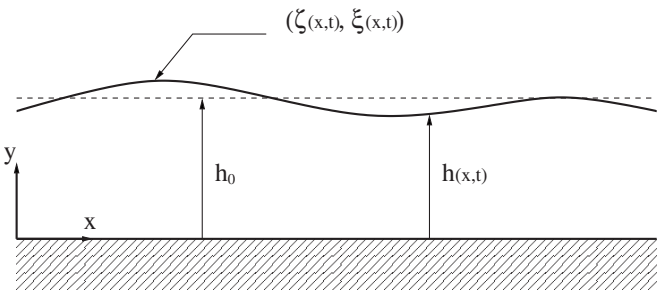

FIG. 1. Two-dimensional thin film of thickness $h(x,t)$ on a horizontal solid substrate. h_0 denotes the flat film thickness. The free surface of the film is covered by a mixture of two chemical species undergoing a chemical reaction with FitzHugh-Nagumo kinetics. The effective concentrations of the two species are $\zeta(x,t)$ and $\xi(x,t)$ with the latter acting as a surfactant. Depending on the values of the physical parameters, the flat film may be unstable exhibiting different types of waves on its surface.

coupled nonlinear partial differential equations for the evolution in time and space of the film thickness profile and the concentration profiles of the two species.

The paper is organized as follows: In Sec. II we formulate the problem mathematically and we outline the governing equations for the coupled hydrodynamic-reaction-diffusion system. In Sec. III we give the governing dimensionless groups and dimensionless governing equations. In Sec. IV we derive a simplified model based on the long-wave approximation. Section V is devoted to the steady state and its linear stability. In Sec. VI, we present theoretical and numerical results on the coupling between chemical fronts, waves and pulses and the convectively evolving free-surface profile of the film. Conclusions and summary are drawn in Sec. VII.

II. PROBLEM DEFINITION AND GOVERNING EQUATIONS

A. Hydrodynamics

We consider a two-dimensional horizontal thin liquid film interacting with chemically reactive insoluble surfactants. Figure 1 sketches the setup. A Cartesian coordinate system (x,y) is chosen so that x is in the direction parallel to the substrate and y is the outward-pointing coordinate normal to the substrate. The fluid has viscosity μ, density ρ, and surface tension σ. The governing equations are the continuity and Navier-Stokes equations,

$$\nabla \cdot \mathbf{u} = 0, \tag{1a}$$

$$\rho\left(\frac{\partial}{\partial t} + \mathbf{u}\cdot\nabla\right)\mathbf{u} = -\nabla p + \nabla\cdot\boldsymbol{\tau} + \rho\mathbf{g}, \tag{1b}$$

where $\nabla=(\partial/\partial x, \partial/\partial y)$ is the gradient operator on the (x,y) plane, $\mathbf{u}=(u,v)$ is the fluid velocity vector, $\mathbf{g}=(0,-g)$, where g is the gravitational acceleration, p is the fluid pressure, and $\boldsymbol{\tau}=\mu[(\nabla\mathbf{u})+(\nabla\mathbf{u})^t]$ is the deviatoric stress tensor.

These equations are subject to the following boundary conditions. On the substrate we have the usual no-slip and no-penetration conditions

$$\mathbf{u} = \mathbf{0} \quad \text{on} \quad y = 0. \tag{2}$$

On the free surface $y=h(x,t)$ we have the kinematic boundary condition along with the normal and tangential stress balances,

$$h_t + uh_x = v,$$

$$-p + (\boldsymbol{\tau}\cdot\mathbf{n})\cdot\mathbf{n} = 2\sigma K(h), \tag{3}$$

$$(\boldsymbol{\tau}\cdot\mathbf{n})\cdot\mathbf{t} = \nabla_s\sigma\cdot\mathbf{t},$$

where without loss of generality the pressure of the surrounding gas phase has been set equal to zero. $\mathbf{n}$ and $\mathbf{t}$ are unit vectors, normal (outward pointing) and tangential to the interface, respectively, defined from $\mathbf{n}=n^{-1}(-h_x,1)$, $\mathbf{t}=n^{-1}(1,h_x)$, where $n=(1+h_x^2)^{1/2}$. $K(h)=-(1/2)\nabla_s\cdot\mathbf{n}$ is the curvature of the interface and $\nabla_s=(\mathbf{I}-\mathbf{nn})\cdot\nabla$ is the surface gradient operator with $\mathbf{I}$ the 2×2 unitary matrix and $\mathbf{nn}$ the dyadic product of the unit vector $\mathbf{n}$ with itself. Hence the tangential stress balance includes the Marangoni effect in its right-hand side through the gradient of the surface tension along the interface.

B. The reaction-diffusion system

We assume an excitable or bistable reaction-diffusion system on the free surface of the film. The state of this excitable or bistable system [referred to also as the chemical (sub)system hereafter] can be described by two variables ζ and ξ corresponding to the concentrations of the two species (actually concentration shifts as we shall discuss later) although they can actually represent linear combinations of concentrations. As discussed in Sec. I, their dynamics is modeled by the FitzHugh-Nagumo system, which has long been used as a prototype system characterized by propagating fronts and pulses.[69] The system can be written in dimensional form as follows:

$$\zeta_t = D_\zeta\zeta_{xx} + k_\zeta(\zeta - b_2'\zeta^3 - b_1'\xi), \tag{4a}$$

$$\xi_t = D_\xi\xi_{xx} + k_\xi(\zeta - a_1'\xi - a_0'). \tag{4b}$$

As no convection is present at this stage, the time evolution of the two chemical species is governed by a set of two reaction-diffusion equations which state that a local change in the chemical system state is due to two main effects: the diffusion of the species on the interface and their generation or consumption by the chemical reaction [first and second term in the right-hand side of Eqs. (4), respectively].

This system is parameterized by eight coefficients, D_ζ and D_ξ are the surface diffusion coefficients of the two species, k_ζ and k_ξ are the reaction rate constants, and a_0', a_1', b_1', and b_2' are the kinetic parameters. All except a_0' are positive. ζ is called the "activator" and ξ the "inhibitor," as discussed in Sec. I; indeed, as can be seen from Eqs. (4), ζ tends to increase the concentration of the species while ξ tends to lower them, hence their names activator/inhibitor. When the ratio k_ζ/k_ξ is large, as is the case for an excitable medium, ζ is a "fast variable" and ξ is a "slow variable." The stationary homogenous solutions of Eqs. (4) (fixed points of the homogenous system) are found by setting all derivatives equal

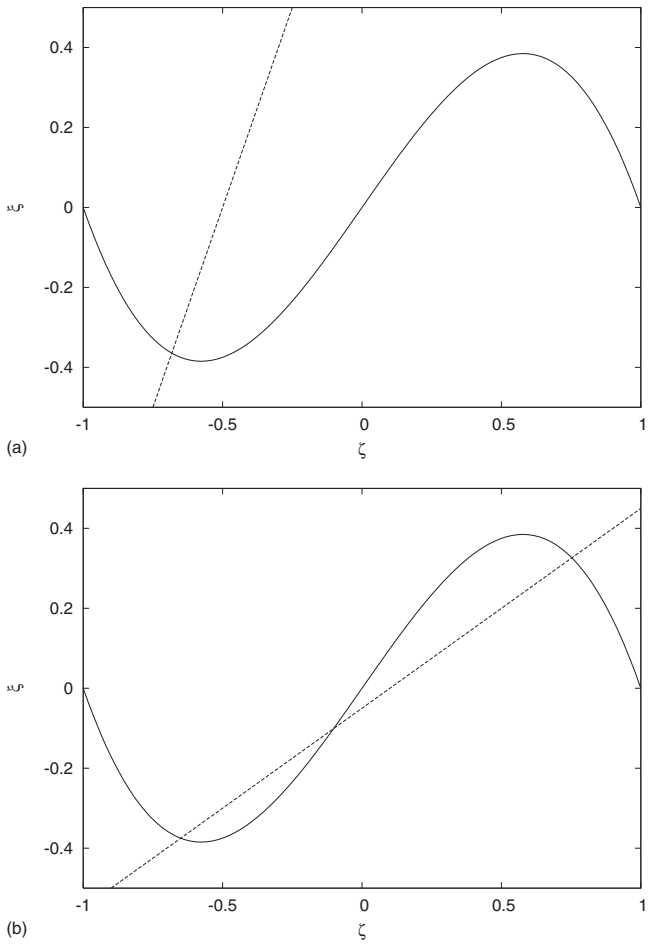

FIG. 2. The nullclines of the FitzHugh-Nagumo equations (4). The intersection points define the homogeneous steady states of the chemical system [Eq. (29)]. (a) Single intersection with $a_0=-0.5$ and $a_1=0.5$ corresponding to the case considered in Figs. 7 and 8. (b) Three intersections with $a_0=0.1$ and $a_1=2.0$ corresponding to the case considered in Fig. 12.

to zero and looking for intersections of the "nullclines," $\zeta - b_2'\xi^3 - b_1'\xi = 0$ and $\zeta - a_1'\xi - a_0' = 0$. The nullclines are depicted in Fig. 2. Depending on the values of a_0', a_1', b_1', and b_2', one or three fixed points exist.

Here we include the effect of convection in the underlying liquid film on the time evolution of the species as it is the first ingredient of the coupling between the flow and the chemical system. To do so, we cannot use Eqs. (4) as it is. Indeed, the FitzHugh-Nagumo equations are in general obtained after a reduction of an initial larger set of equations, so that ζ and ξ, whose physical meaning may be lost in the reduction process, do not necessarily correspond to the physical variables that are actually transported by the flow. Hence there is a need to distinguish between the actual values of the species concentrations, denoted ζ' and ξ', in terms of which the transport equations should be formulated, and the variables ζ and ξ that appear in the kinetic terms of the FitzHugh-Nagumo equations. We then suppose that in this model there is a simple connection between them, i.e., $\zeta' = \zeta + \zeta_m'$ and $\xi' = \xi + \xi_m'$. This way ζ and ξ refer to the *deviations* of the actual concentrations from their reference values, denoted as ζ_m' and ξ_m', respectively. Further, the values of ζ_m' and ξ_m' can ensure positivity of the variables ζ' and ξ' which is essential if these variables are to describe actual species transported by the flow [Eq. (4) admits negative values for ζ and ξ; notice, e.g., the symmetry $(\xi,\zeta)\to(-\xi,-\zeta)$ for $a_0'=0$]. If $\zeta_m'=\xi_m'=0$ and ζ, ξ are negative, then these variables do not represent actual concentrations, but something more involved, e.g., linear combinations of concentrations.

We then suppose that the kinetic parts included in the transport equations for ξ' and ζ' may be written in the following form, which incorporates a total of eight parameters:

$$F_1(\zeta',\xi') = k_\zeta[\zeta' - \zeta_m' - b_2'(\zeta' - \zeta_m')^3 - b_1'(\xi' - \xi_m')], \quad (5a)$$

$$F_2(\zeta',\xi') = k_\xi[(\zeta' - \zeta_m') - a_1'(\xi' - \xi_m') - a_0']. \quad (5b)$$

The values of ζ_m' and ξ_m', along with those of k_ζ, k_ξ, a_0', a_1', b_1', and b_2', are given by the actual excitable/bistable system under consideration.

C. The surface transport equations

We first obtain the basic surface transport equation in the absence of chemical reaction and surface diffusion. Amongst the several studies that dealt with this issue before, we note the works by Stone,[70] Wong *et al.*,[71] and Cermelli *et al.*[72] The last two derived the transport equation from different starting points to that in Ref. 70, pointing out the ambiguity of the time derivative in the equation given there and providing the proper interpretation of this derivative as the time derivative in a direction normal to the interface. Here, we offer a simple and concise derivation of the basic surface transport equation using the same starting point as Ref. 70. Our derivation parallels in part Ref. 70 but also clearly provides the proper interpretation of the time derivative used in Ref. 70.

Let Γ denote the concentration per unit area of a chemical species on the free surface. Our starting point is Eqs. (2) and (4) in Ref. 70: if S denotes a two-dimensional curved surface, the conservation of species can be simply expressed by $D/Dt\int_S \Gamma dS = 0$, where D/Dt is the Lagrangian derivative. This expression can be written as

$$\int_S \left(\frac{D\Gamma}{Dt} dS + \Gamma \frac{D}{Dt} dS \right) = 0, \quad (6)$$

corresponding to Eq. (2) of Ref. 70. The Lagrangian derivative of dS can be expressed in terms of the surface gradient of the velocity field $\mathbf{u}$ at the surface through Eq. (4) of Ref. 70 (which in turn originates from Batchelor's book[73]), rewritten here for clarity,

$$\frac{D}{Dt} dS = dS \boldsymbol{\nabla}_s \cdot \mathbf{u}, \quad (7)$$

where $\boldsymbol{\nabla}_s$ is the surface gradient operator defined in Sec. II A. Combining Eqs. (6) and (7), and since S is an arbitrary surface element, one gets

$$\frac{D\Gamma}{Dt} + \Gamma \boldsymbol{\nabla}_s \cdot \mathbf{u} = 0, \quad (8)$$

our basic surface transport equation in the absence of reaction and surface diffusion. Note that the term $\Gamma \boldsymbol{\nabla}_s \cdot \mathbf{u}$ ac-

counts for the change of the concentration due to the stretching of the interface.

From the definition now of the Lagrangian derivative, $D\Gamma/Dt=\partial\tilde{\Gamma}/\partial t+(\mathbf{u}\cdot\boldsymbol{\nabla})\tilde{\Gamma}$, where we have implicitly extended the surface field Γ to a two-dimensional neighborhood of the interface, $\tilde{\Gamma}$, as Cermelli *et al.*[72] did in their study. Clearly by doing so, the individual terms $\partial\tilde{\Gamma}/\partial t$ and $(\mathbf{u}\cdot\boldsymbol{\nabla})\tilde{\Gamma}$ might depend on the particular extension being employed, however our derivation does not depend on the extension as long as the two terms are kept together (which they are) since their sum, $D\Gamma/Dt$, does not depend on the extension. We then obtain from Eq. (8)

$$\frac{\partial\tilde{\Gamma}}{\partial t}+(\mathbf{u}\cdot\boldsymbol{\nabla})\tilde{\Gamma}+\Gamma\boldsymbol{\nabla}_s\cdot\mathbf{u}=0. \tag{9}$$

By decomposing $\mathbf{u}$ in the term $\mathbf{u}\cdot\boldsymbol{\nabla}$ of Eq. (9) into two components, a normal to the surface, $\mathbf{u}_n$, and a tangential to the surface, $\mathbf{u}_s$, Eq. (9) can be written as

$$\frac{\partial\tilde{\Gamma}}{\partial t}+(\mathbf{u}_s\cdot\boldsymbol{\nabla})\tilde{\Gamma}+(\mathbf{u}_n\cdot\boldsymbol{\nabla})\tilde{\Gamma}+\Gamma\boldsymbol{\nabla}_s\cdot\mathbf{u}=0, \tag{10}$$

which by utilizing the relationships $\mathbf{u}_s\cdot\boldsymbol{\nabla}=\mathbf{u}\cdot\boldsymbol{\nabla}_s$ and $(\mathbf{u}\cdot\boldsymbol{\nabla}_s)\Gamma+\Gamma(\boldsymbol{\nabla}_s\cdot\mathbf{u})=\boldsymbol{\nabla}_s\cdot(\Gamma\mathbf{u})$ can be written as

$$\frac{\partial\tilde{\Gamma}}{\partial t}+(\mathbf{u}_n\cdot\boldsymbol{\nabla})\tilde{\Gamma}+\boldsymbol{\nabla}_s\cdot(\Gamma\mathbf{u})=0. \tag{11}$$

Note that the sum of the first two terms does not depend on the particular extension as the third term involves only $\boldsymbol{\nabla}_s$. At first this equation appears to differ from Eq. (5) of Ref. 70, which does not contain the contribution of the normal component, $(\mathbf{u}_n\cdot\boldsymbol{\nabla})\tilde{\Gamma}$. However, the transformation $\partial\tilde{\Gamma}/\partial t+(\mathbf{u}_n\cdot\boldsymbol{\nabla})\tilde{\Gamma}\rightarrow\partial\Gamma/\partial t$ in Eq. (11) gives precisely Eq. (5) in Ref. 70. Therefore, the partial time derivative in Ref. 70 should not be interpreted as the usual partial time derivative, i.e., the derivative obtained by differentiating with respect to time for a fixed point in space, and hence the time derivative in the laboratory frame, but as the partial time derivative that follows the interface in a direction normal to the interface (this time derivative was referred to by Cermelli *et al.*[72] as the "normal time derivative following the surface"). The same conclusion was reached by Wong *et al.*,[71] who also obtained the surface transport equation in an arbitrary surface coordinate system, and by Cermelli *et al.*[72] who extensively discussed the role of the normal time derivative following the surface in the description of evolving interfaces (the same study offers a detailed analysis of transport relations for surface integrals over evolving interfaces including applications to surfactant transport). Hence, unlike Ref. 70, where the surface transport equation is written in a frame of reference moving with the velocity normal to the interface, here the surface transport equation is written in the laboratory frame of reference, a frame more appropriate for the description of interfacial waves.

We now return to Eq. (8). As we shall discuss in Sec. IV, in the present study we shall be concerned with long waves thus excluding the possibility of multivalued interfaces. Hence Γ is allowed to be a function of x and we can use the one-dimensional version of the Lagrangian derivative, $D\Gamma/Dt=\partial\Gamma/\partial t+u\Gamma_x$, so that Eq. (8) can be further simplified to

$$\frac{\partial\Gamma}{\partial t}+u\Gamma_x+\Gamma\boldsymbol{\nabla}_s\cdot\mathbf{u}=0. \tag{12}$$

Note that this equation can also be derived by using Eq. (9), where for the sake of simplicity the following extension for Γ may be chosen: $\tilde{\Gamma}(x,y,t)\equiv\Gamma(x,t)$, i.e., $\tilde{\Gamma}$ does not depend on y. With $\Gamma=\zeta',\xi'$ now and adding to the right-hand side of Eq. (12) the diffusive contributions $D_\Gamma\nabla_s^2\Gamma$ with D_Γ a surface diffusion coefficient and the source contributions from the kinetic terms in Eqs. (5a) and (5b), we obtain the following transport equations at $y=h(x,t)$ for the two species:

$$\zeta_t+u\zeta_x+(\zeta_m'+\zeta)\boldsymbol{\nabla}_s\cdot\mathbf{u}=D_\zeta\nabla_s^2\zeta+k_\zeta(\zeta-b_2'\zeta^3-b_1'\xi) \tag{13a}$$

$$\xi_t+u\xi_x+(\xi_m'+\xi)\boldsymbol{\nabla}_s\cdot\mathbf{u}=D_\xi\nabla_s^2\xi+k_\xi(\zeta-a_1'\xi-a_0'). \tag{13b}$$

From our earlier discussion, the first two terms in the left-hand sides of the above equations correspond to the Lagrangian derivatives of the concentrations of the two species, while the third terms account for the changes due to the stretching of the interface.

The interaction between the flow and the chemical system takes place in two ways. On the one hand, the flow changes the distribution of the species at the film surface by convection. On the other hand, the chemical system acts upon the surface through the surface tension. The system is then closed by expressing the surface tension as a function of concentration. For simplicity we assume that only the inhibitor acts as a surfactant and alters the surface tension. Further, the dependence of σ on ξ is supposed to be sufficiently weak to justify an expansion of σ in ξ around ξ_m'. We then define $\sigma_m=\sigma(\xi_m')$ and γ by

$$\sigma(\xi_m'+\xi)=\sigma_m-\gamma\xi, \tag{14}$$

which allows the evaluation of the right-hand side of the tangential stress balance in Eqs. (3). $\gamma>0$ for typical liquids while σ_m is assumed to be sufficiently large so that moderate values of ξ do not lead to unphysical negative surface tensions.

III. SCALINGS AND DIMENSIONLESS EQUATIONS

The vertical scale is the undisturbed film thickness h_0. The horizontal scale ℓ is a typical length of the pattern appearing at the film surface. Any pattern on the free surface is driven by the chemical system and hence ℓ is determined by the chemical system, more precisely by the activator ξ which acts as a surfactant as noted earlier. Likewise, the characteristic velocity U in the horizontal direction is set by ξ so that the characteristic time scale is obtained from ℓ/U (unlike the reactive falling film problem in Refs. 57–59, where the flow is due to gravity so that the dynamics is driven by the hydrodynamics and all scales were based on the hydrodynamics). We then introduce the nondimensionalization

$$x \to \ell\, x, \quad (y,h) \to h_0(y,h), \quad t \to \frac{\ell}{U}t, \tag{15a}$$

$$u \to Uu, \quad v \to \frac{Uh_0}{\ell}v, \quad p \to \frac{\mu U \ell}{h_0^2}p,$$

$$\zeta \to \zeta^* \zeta, \quad \xi \to \xi^* \xi, \tag{15b}$$

where

$$\ell = \sqrt{\frac{D_\xi}{k_\xi}\frac{\xi^*}{\zeta^*}}, \quad U = \sqrt{D_\xi k_\xi \frac{\zeta^*}{\xi^*}}, \quad \zeta^* = \frac{1}{\sqrt{b_2'}}, \quad \xi^* = \frac{\zeta^*}{b_1'}. \tag{16}$$

In terms of the above nondimensionalization, the continuity and Navier-Stokes equations in Eqs. (1) become

$$u_x + v_y = 0, \tag{17a}$$

$$\varepsilon\,\mathrm{Re}(u_t + uu_x + vu_y) = -p_x + \varepsilon^2 u_{xx} + u_{yy}, \tag{17b}$$

$$\varepsilon^3\,\mathrm{Re}(v_t + uv_x + vv_y) = -p_y + \varepsilon^4 v_{xx} + \varepsilon^2 v_{yy} - \varepsilon\,\mathrm{Bo}. \tag{17c}$$

These equations are subject to the wall boundary conditions

$$u = v = 0 \quad \text{on} \quad y = 0, \tag{18}$$

and the dimensionless versions of the interfacial boundary conditions in Eqs. (3)

$$h_t + uh_x = v, \tag{19a}$$

$$p + \frac{2\varepsilon^2}{1+\varepsilon^2 h_x^2}[(1-\varepsilon^2 h_x^2)u_x + h_x(u_y + \varepsilon^2 v_x)] = -\varepsilon^3(\mathrm{We} - \mathrm{Ma}\,\xi)\frac{h_{xx}}{(1+\varepsilon^2 h_x^2)^{3/2}}, \tag{19b}$$

$$-4\varepsilon^2 h_x u_x + (1-\varepsilon^2 h_x^2)(u_y + \varepsilon^2 v_x) = -\sqrt{1+\varepsilon^2 h_x^2}\,\varepsilon\,\mathrm{Ma}\,\xi_x. \tag{19c}$$

On the interface we also have the following dimensionless versions of the surface transport equations in Eqs. (13):

$$\zeta_t + u\zeta_x + \frac{\zeta_m + \zeta}{1+\varepsilon^2 h_x^2}[(u_x + \varepsilon^2 h_x v_x) + h_x(u_y + \varepsilon^2 h_x v_y)] = \frac{1}{\delta}\left(\frac{\zeta_{xx}}{1+\varepsilon^2 h_x^2} - \varepsilon^2 \frac{\zeta_x h_x h_{xx}}{(1+\varepsilon^2 h_x^2)^2}\right) + K(\zeta - \zeta^3 - \xi) \tag{20a}$$

and

$$\xi_t + u\xi_x + \frac{\xi_m + \xi}{1+\varepsilon^2 h_x^2}[(u_x + \varepsilon^2 h_x v_x) + h_x(u_y + \varepsilon^2 h_x v_y)] = \frac{\xi_{xx}}{1+\varepsilon^2 h_x^2} - \varepsilon^2 \frac{\xi_x h_x h_{xx}}{(1+\varepsilon^2 h_x^2)^2} + (\zeta - a_1\xi - a_0). \tag{20b}$$

The different dimensionless groups and parameters in the above system of equations are defined as follows:

$$\mathrm{Re} = \frac{\rho U h_0}{\mu}, \quad \mathrm{Bo} = \frac{\rho g h_0^2}{\mu U}, \quad \mathrm{We} = \frac{\sigma_m}{\mu U}, \quad \mathrm{Ma} = \frac{\gamma \xi^*}{\mu U}, \quad \varepsilon = \frac{h_0}{\ell}, \tag{21a}$$

$$\delta = \frac{D_\xi}{D_\zeta}, \quad K = \frac{\xi^*}{\zeta^*}\frac{k_\zeta}{k_\xi}, \quad \zeta_m = \frac{\zeta_m'}{\zeta^*}, \quad \xi_m = \frac{\xi_m'}{\xi^*}, \quad a_0 = \frac{a_0'}{\zeta^*}, \quad a_1 = a_1'\frac{\xi^*}{\zeta^*}. \tag{21b}$$

Re is the Reynolds number, Bo is the Bond number, We is the Weber number, Ma is the Marangoni number, and ε is the aspect ratio or "film parameter" as is frequently called in thin film studies.[74] The last six groups are related to the chemical system only.

IV. LONG-WAVE EXPANSION

We shall not investigate the dynamics of the full system in Eqs. (17)–(20), but rather restrict our attention to long-wave surface dynamics, i.e., slow time and space variations of the flat film. The y-dependence of the system in Eqs. (17)–(20) can then be suppressed and its complexity thereby greatly reduced. For the long-wave approximation we must ensure that the length scale of the waves propagating on the film surface is large compared to the film thickness, i.e., $\varepsilon \ll 1$. Since the typical length scale of the interfacial waves and of the ξ-waves is of the same order as we pointed out in the previous section, both h and ξ are "long-wave" variables. The length scale of ζ is discussed below.

We now assume the following relative orders between the dimensionless groups that affect the hydrodynamics and the film parameter ε: $\mathrm{Re}=\mathcal{O}(1)$ (lubrication approximation), $\mathrm{Bo}=\mathcal{O}(1/\varepsilon)$, $\mathrm{We}=\mathcal{O}(1/\varepsilon^3)$, and $\mathrm{Ma}=\mathcal{O}(1/\varepsilon)$. With the orders of magnitude assignments for Bo, We, and Ma we include the different physical effects at the lowest possible order, i.e., at $\mathcal{O}(1)$. For convenience we introduce the following modified parameters: $B=\varepsilon\,\mathrm{Bo}$, $W=\varepsilon^3\,\mathrm{We}$, and $M=\varepsilon\,\mathrm{Ma}$, which are all $\mathcal{O}(1)$.

For the chemical system parameters δ and K we do not assign an order with respect to ε. After all the long-wave approximation affects the hydrodynamics, the convective parts of the surface transport equations and the diffusive terms of these equations through the surface gradient operator but not the kinetic term $K(\zeta-\zeta^3-\xi)$ and the spatial derivative $(1/\delta)\xi_{xx}$ in the surface transport equation for ζ which determine the wavelength of ζ with respect to ξ. Let us consider, e.g., the case of fronts for the pure chemical system. By appropriately choosing the parameters δ and K one can have "sharp" or smooth fronts for ζ but always smooth or "long-wave" fronts for ξ (the two variables are coupled and clearly changing δ and K affects the shape of ξ but not the order of magnitude of its wavelength). Indeed, computations with, e.g., $K=10$ and $\delta=1$ reveal a sharper front for ζ compared to that for ξ while reducing K to, e.g., 0.1 and maintaining δ the same makes ζ a long-wave front. Computations with, e.g., $\delta=100$ and $K=0.1$ give results similar to those with $K=10$ and $\delta=1$, i.e., ζ is long and ξ is sharp. So the

ζ-front can be made sharp either by increasing K for a fixed δ or by increasing δ for a fixed K. It turns out that the same is true for the coupled system, i.e., changing δ and K alters the wavelength of ζ leading to sharper fronts for large δ and/or large K. Now ξ is always a long-wave variable with respect to the film parameter ε. On the other hand, had we coupled the hydrodynamics to ζ instead of ξ, the long-wave assumption would make ζ long while the wavelength of ξ would depend on the values of δ and K and would vary from being of the same order with that of ζ to being much longer.

Retaining now only the leading-order terms for the hydrodynamic system in Eqs. (17)–(19) yields

$$u_x + v_y = 0, \tag{22a}$$

$$p_x = u_{yy}, \tag{22b}$$

$$p_y = -B, \tag{22c}$$

subject to the wall boundary conditions

$$u = 0, \quad v = 0, \tag{23}$$

and free-surface boundary conditions $[y=h(x,t)]$

$$h_t + uh_x - v = 0, \tag{24a}$$

$$p = -Wh_{xx}, \tag{24b}$$

$$u_y = -M\xi_x, \tag{24c}$$

while the leading-order terms of the surface transport equations in Eqs. (20) give

$$\zeta_t + [u(\zeta_m + \zeta)]_x = \frac{1}{\delta}\zeta_{xx} + K(\zeta - \zeta^3 - \xi) \tag{25a}$$

and

$$\xi_t + [u(\xi_m + \xi)]_x = \xi_{xx} + \zeta - a_1\xi - a_0 \tag{25b}$$

at $y=h(x,t)$. The leading-order terms of the horizontal velocity and pressure field are then easily determined from Eqs. (22b), (22c), (24b), and (24c). They read

$$p = B(h - y) - Wh_{xx} \tag{26}$$

and

$$u = (Bh - Wh_{xx})_x y\left(\tfrac{1}{2}y - h\right) - M\xi_x y, \tag{27}$$

respectively. Using Eqs. (22a) and (23), the leading-order term of the vertical velocity v is easily determined. Substituting u and v into the kinematic boundary condition (24a) and u into the surface transport equations (25) yields a set of three coupled nonlinear partial differential equations for the evolution in time and space of the fields h, ζ, and ξ,

$$h_t = \left(\frac{1}{3}Bh^3h_x - \frac{1}{3}Wh^3h_{xxx} + \frac{1}{2}Mh^2\xi_x\right)_x, \tag{28a}$$

$$\zeta_t = \left(\frac{1}{2}Bh^2(\zeta_m + \zeta)h_x - \frac{1}{2}Wh^2(\zeta_m + \zeta)h_{xxx} + Mh(\zeta_m + \zeta)\xi_x\right)_x + \frac{1}{\delta}\zeta_{xx} + K(\zeta - \zeta^3 - \xi), \tag{28b}$$

and

$$\xi_t = \left(\frac{1}{2}Bh^2(\xi_m + \xi)h_x - \frac{1}{2}Wh^2(\xi_m + \xi)h_{xxx} + Mh(\xi_m + \xi)\xi_x\right)_x + \xi_{xx} + \zeta - a_1\xi - a_0. \tag{28c}$$

These are the basic equations for the analysis to follow. They account for the coupling of the two subsystems: the free surface dynamics of the thin film and the excitable/bistable reaction-diffusion system.

V. ANALYSIS OF THE UNIFORM STATE

Depending on the values of a_0 and a_1, Eqs. (28) have one or three uniform steady solutions obtained by setting the time and space derivatives in these equations equal to zero. They are defined by the flat film solution $h=1$ and the values $\zeta=\zeta_0$, and $\xi=\xi_0$ obtained from the solution of the following algebraic system:

$$\zeta_0 - \zeta_0^3 - \xi_0 = 0, \tag{29a}$$

$$\zeta_0 - a_1\xi_0 - a_0 = 0. \tag{29b}$$

Hence the values ζ_0 and ξ_0 coincide with those obtained from the nullclines of the pure reaction-diffusion system defined in Sec. II B (Fig. 2). We now analyze the temporal linear stability of these states focusing on the influence of the modified Marangoni number.

Linearization of Eqs. (28) around $(1,\zeta_0,\xi_0)$ yields

$$h_t = \frac{1}{3}Bh_{xx} - \frac{1}{3}Wh_{xxxx} + \frac{1}{2}M\xi_{xx}, \tag{30a}$$

$$\zeta_t = \frac{1}{2}B(\zeta_m + \zeta_0)h_{xx} - \frac{1}{2}W(\zeta_m + \zeta_0)h_{xxxx} + M(\zeta_m + \zeta_0)\xi_{xx} + \frac{1}{\delta}\zeta_{xx} - K\beta\zeta - K\xi, \tag{30b}$$

and

$$\xi_t = \frac{1}{2}B(\xi_m + \xi_0)h_{xx} - \frac{1}{2}W(\xi_m + \xi_0)h_{xxxx} + M(\xi_m + \xi_0)\xi_{xx} + \xi_{xx} + \zeta - a_1\xi. \tag{30c}$$

Introducing the normal modes $(h,\zeta,\xi)=(H,Z,X)\exp(\lambda t + ikx)$, where k is the real wavenumber and λ the complex growth rate, yields a linear algebraic system with constant coefficients. For the system to have nontrivial solutions it is necessary and sufficient that its principal determinant be equal to zero. This yields an algebraic eigenvalue problem of the form $\det\|\mathbf{A}-\lambda\mathbf{I}\|=0$, where $\mathbf{A}$ is a 3×3 matrix and $\mathbf{I}$ is the unitary matrix. This is a cubic equation for the dispersion relation $\lambda=\lambda(k)$,

$$\lambda^3 + p\lambda^2 + q\lambda + r = 0, \tag{31a}$$

where

$$p = K\beta + \frac{k^2}{\delta} + (M_\xi + 1)k^2 + a_1 + \frac{k^2}{3}(B + Wk^2), \tag{31b}$$

$$q = \left(K\beta + \frac{k^2}{\delta}\right)[(M_\xi + 1)k^2 + a_1] + K + M_\zeta k^2 + \frac{k^2}{3}(B + Wk^2)\left[K\beta + \left(\frac{1}{\delta} + \frac{M_\xi}{4} + 1\right)k^2 + a_1\right], \tag{31c}$$

and

$$r = \frac{k^2}{3}(B + Wk^2)\left\{\left(K\beta + \frac{k^2}{\delta}\right)\left[\left(\frac{M_\xi}{4} + 1\right)k^2 + a_1\right] + K + \frac{1}{4}M_\zeta k^2\right\}, \tag{31d}$$

and where, for convenience, we have introduced the new dimensionless parameters,

$$\beta = 3\zeta_0^2 - 1, \quad M_\zeta = (\zeta_m + \zeta_0)M, \quad \text{and} \quad M_\xi = (\xi_m + \xi_0)M. \tag{31e}$$

Note that all coefficients in Eqs. (31b)–(31d) are even in k. As a consequence λ in Eq. (31a) is also even in k, a manifestation of the reflection symmetry $x \to -x$ of the system. Further, note that for $k=0$, $r=0$ and hence one eigenvalue, say λ_1, vanishes. Let $[H_i Z_i X_i]^t$ denote the eigenvector corresponding to the eigenvalue λ_i. It turns out that $[H_1 Z_1 X_1]^t$ is such that $H_1 \neq 0$ for $k=0$. The eigenvalue $\lambda_1 = 0$ for $k=0$ originates from the hydrodynamic equation (30a) followed by the substitution of normal modes: in this limit $\lambda_1 H_1 = 0$ or $\lambda_1 = 0$. It also turns out that the first components H_2, H_3 of the other two eigenvectors vanish for $k=0$. Hence for the special case $k=0$ the chemical subsystem does not affect the hydrodynamic subsystem and at the same time since $\lambda_1 = 0$ originates from the hydrodynamic equation (30a) the hydrodynamic subsystem is always neutrally stable in this limit.

If all dimensionless parameters in the coefficients (31b)–(31d) are strictly positive, $p > 0$, $pq > r$, and $r > 0$. According to the Hurwitz-Routh criterion then, the real parts of all the roots of Eq. (31a) are strictly negative and the corresponding uniform steady state is linearly stable. A destabilization of the whole system may nevertheless occur if, for example, the values of ζ_m and ξ_m are such that M_ζ and/or M_ξ are negative or if the modified Marangoni number M is negative. Note that, although surface tension typically decreases with concentration, there are several systems which are known to display the opposite behavior.[75] Another possibility, due to the excitable/bistable system, is the case $\beta < 0$.

In the case $M=0$, much like the limit $k=0$ discussed above, the chemical subsystem does not affect the hydrodynamics. For $M=0$ the Marangoni effect is eliminated but convection can still be present. Clearly the free surface is linearly stable as the dispersion relation for the hydrodynamic system $\lambda = -(k^2/3)(B + Wk^2)$ from Eq. (30a) shows that any disturbance on it will decay for large times. Similarly, the u-velocity would vanish for large times as is evident from Eq. (27). For earlier times, however, there would be a transient regime with nonzero free-surface gradients leading also to a nonzero u-velocity which would then influence the concentrations of both species through the convective term in the left-hand side of Eqs. (25a) and (25b) or their equivalent expressions in Eq. (28c). Hence we never have a truly decoupled system; that would correspond to the case, where both Marangoni effect and convection are absent.

Let us now investigate in detail the linear stability characteristics for $M=0$. In this case Eq. (31a) can be factorized,

$$\left[\lambda + \frac{k^2}{3}(B + Wk^2)\right] \times \left[\lambda^2 + \left(K\beta + \frac{k^2}{\delta} + k^2 + a_1\right)\lambda + \left(K\beta + \frac{k^2}{\delta}\right)(k^2 + a_1) + K\right] = 0, \tag{32}$$

where the first factor is associated with h and the second one accounts for the chemical subsystem. This factorization is possible because for $M=0$ the chemical subsystem does not affect the free surface, even though there is still an influence of the hydrodynamics on the chemical system through convection, as discussed above. Equation (32) reveals that for $M=0$, the two subsystems have in general different behaviors: the uniform free surface is always linearly stable while the chemical subsystem can be stable or unstable. A necessary condition for instability is that $\beta < 0$, as β is the only parameter that can change sign and becomes from positive to negative. Since β corresponds to the negative slope of the nullcline $\xi_0(\zeta_0)$ given by Eq. (29a), the unstable steady state of the chemical subsystem is located on the inner solution branch of Eq. (29a) (see Fig. 2). A general sufficient and necessary condition for instability can be obtained from the second factor of Eq. (32) (the specific case $a_0 = 0$ is treated in Ref. 69). The spatially uniform steady state of the chemical subsystem is unstable when at least one of the two conditions,

$$\beta < -\min(1/a_1, a_1/K) \tag{33a}$$

and

$$\beta K\delta < a_1 - \max(2a_1, 2\sqrt{K\delta}), \tag{33b}$$

is satisfied. The destabilization occurs through a Hopf (at onset the growth rate is purely imaginary) or a "Turing bifurcation" (see Fig. 4). The term Turing bifurcation is specific to reaction-diffusion systems and means that a spatially homogeneous state becomes linearly unstable to a spatial pattern at a critical value of a (bifurcation) parameter.[76] The growth rate is real and for values of the bifurcation parameter larger than the critical one the dispersion curve for the growth rate as a function of wavenumber is characterized by a band of unstable wavenumbers centered around the most unstable mode $k_{\max}$ and bounded by two neutral wavenumbers $k_{1,2}$ such that $0 < k_1 < k_{\max} < k_2$. The fully nonlinear system demonstrates the existence of a stationary periodic pattern of wavenumber $k_{\max}$, a "Turing pattern." In the present case, if

$$-\min(1/a_1, a_1/K) < \beta < 0 \quad \text{and} \quad \beta \geq -1, \tag{34}$$

the spatially uniform steady state of the chemical subsystem undergoes a Turing instability as soon as $\delta > \delta_c$, where the critical value δ_c is defined by

$$\sqrt{K\delta_c} = -\frac{1}{\beta}(1 + \sqrt{1 + \beta a_1}). \tag{35}$$

The maximum growing wavenumber at criticality is then given by

$$k_{\max,c} = \sqrt{\sqrt{K\delta_c} - a_1}. \tag{36}$$

In all other cases, the destabilization occurs with $k_{\max,c}=0$. In the case of a Hopf bifurcation this results in an oscillatory behavior in time but uniform in space.

Next, we examine how the stability of the homogeneous steady states is influenced by the coupling, i.e., by a nonzero modified Marangoni number. Two different situations are encountered.

Case I: The excitable/bistable subsystem in the absence of hydrodynamics is unstable, i.e., one of the conditions in Eqs. (33) is fulfilled. Then it is to be expected that at least for weak coupling the full system is also linearly unstable, i.e., the free surface is destabilized. Two typical examples are presented in Fig. 3 (case Ia) and Fig. 4 (case Ib). Both dispersion curves exhibit a range of unstable wavenumbers corresponding to modes with a complex [Fig. 3(a); Hopf bifurcation at onset corresponding to a solution that oscillates in time but is uniform in space] or a real growth rate [Fig. 4(a)]. For the case of real growth rate the dispersion curves are reminiscent of Turing-type dispersion curves but we refrain from using the term "Turing instability" discussed earlier. Of course there are several systems in addition to reaction-diffusion systems (such as reactive flows in Hele-Shaw cells[54,55]) with Turing-type dispersion curves and in which the nonlinearities saturate the linear instability leading to spatially periodic stationary structures. However, there are also several systems, e.g., channel flow and Blasius boundary layer[77] which do not equilibrate to stationary norm solutions. The issue of whether or not an instability saturates to a stationary norm state is essentially a nonlinear question. Indeed we shall demonstrate through fully nonlinear computations that at least in the region of the parameter space we have explored, a Turing pattern for the coupled system is not observed despite the Turing-type dispersion curves. When the growth rate is complex and hence the primary bifurcation is of the Hopf-type, the instability onset is characterized by periodic oscillations in time. Again, the behavior of the system far from criticality can only be addressed through fully nonlinear computations.

By increasing now the modified Marangoni number M the instability is weakened and eventually for sufficiently large M the instability can be suppressed all together. In case Ia, the dominant mode is $k=0$ and as we have seen earlier, this mode corresponds to the case where the chemical system does not affect the hydrodynamics. Hence this mode is not affected by the modified Marangoni number. However, the range of unstable modes around $k=0$ is shortened by the Marangoni stresses: for large wavelength modes the spatial

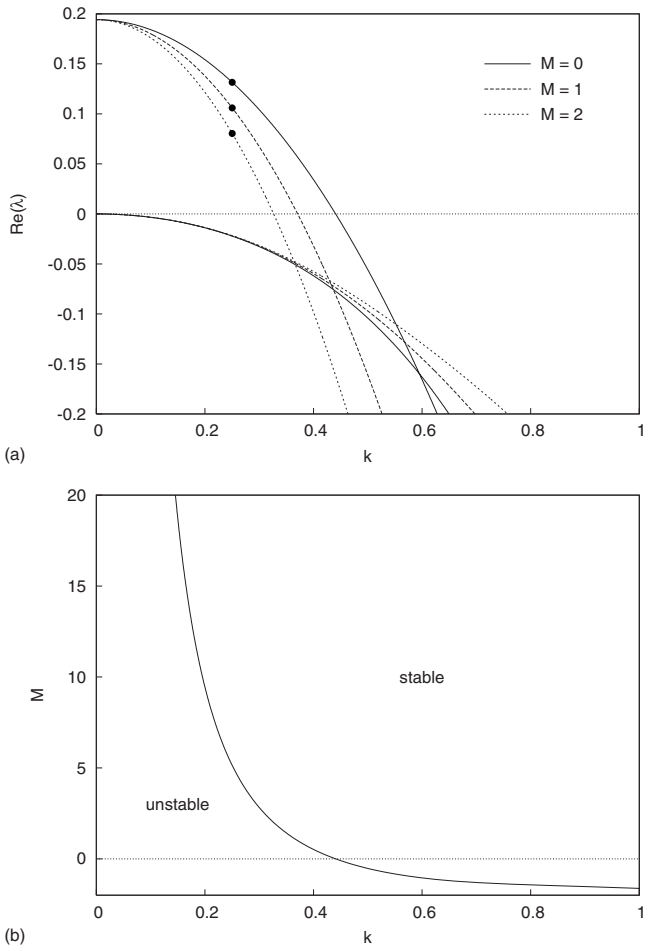

FIG. 3. Case Ia for $\delta=1$, $K=1$, $\zeta_m=1$, $\xi_m=1$, $a_0=-0.1$, $a_1=0.5$, $B=1$, and $W=1$. (a) Dispersion curves for $M=0$ (solid lines), $M=1$ (dashed lines), and $M=2$ (dotted lines). As the modified Marangoni number increases, the range of unstable modes becomes smaller. A bullet (•) on a curve indicates that for this curve the growth rate is complex. Only two growth rates for each M are shown; the third one is the complex conjugate of the complex growth rate. (b) Corresponding stability map.

gradients in the concentrations generate Marangoni flows which tend to homogenize the species on the surface and stabilize the chemical subsystem. In case Ib, the instability can even be suppressed by the hydrodynamics [Fig. 4(b)] although no dramatic change is observed in the shape of the dispersion curves [Fig. 4(a)]. Here the behavior of the system can be understood by considering the two opposing forces acting on it. The intrinsic dynamics of the chemical subsystem, as a reaction diffusion system, tends to generate a spatially periodic stationary pattern. Gradients in the species concentrations arise and induce a gradient of the surface tension and, accordingly, a Marangoni flow [Fig. 5(b)]. At the same time, the convective flow tends to homogenize the species on the surface. As a result, for moderate modified Marangoni numbers we can have finite-amplitude steady solutions for all fields, h, ζ, and ξ. They are computed using the continuation software AUTO97 (Refs. 78–80) and imposing periodic boundary conditions in the domain $[0,1]$ close to the maximum growing wavenumber of $\simeq 2\pi$ as Fig. 4 indicates. These solutions result from the balance of the two processes described above and are depicted in Figs. 5(a) and

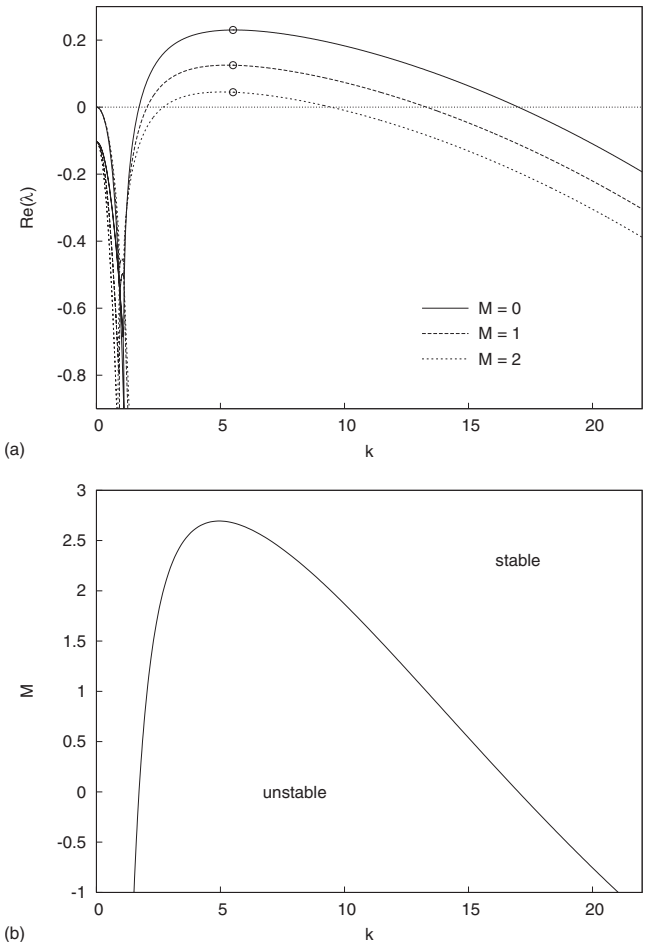

FIG. 4. Case Ib, defined by $\delta=1000$, $K=1$, $\zeta_m=1$, $\xi_m=1$, $a_0=-0.3$, $a_1=0.5$, $B=1$, and $W=1$. (a) Dispersion curves for $M=0$ (solid lines), $M=1$ (dashed lines), and $M=2$ (dotted lines). As in Fig. 3, the Marangoni stresses shorten the range of unstable modes. A circle (◦) on a curve indicates that for this curve the growth rate is real. (b) Corresponding stability map.

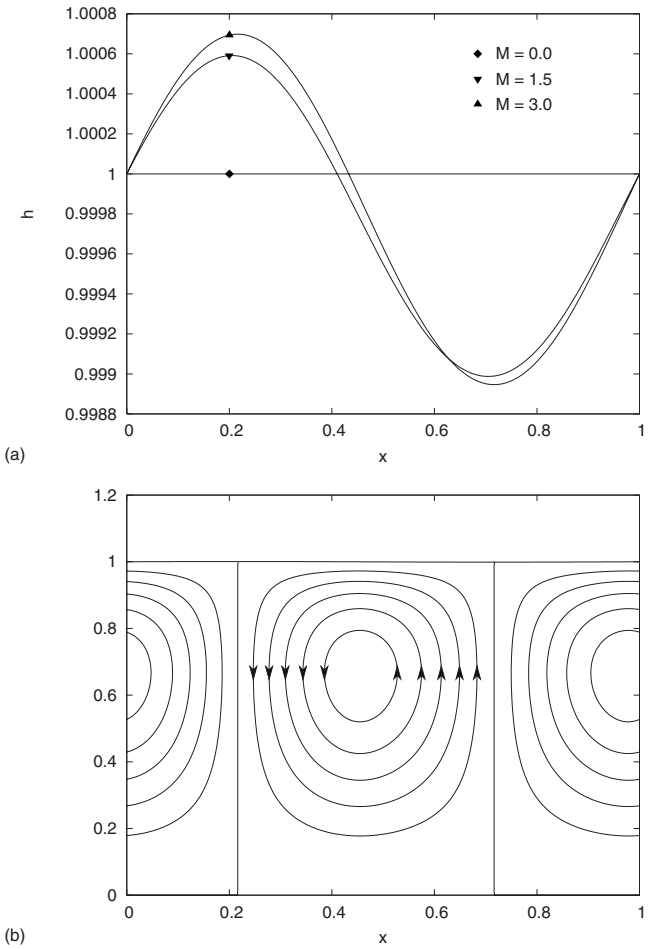

FIG. 5. Case Ib (cf. Fig. 4). (a) Free-surface profile h for different values of the modified Marangoni number: $M=0$, 1.5, and 3. (b) Corresponding streamlines for $M=3$. The flow induced by the Marangoni stresses gives rise to a stationary pattern for the film surface.

6. However, these spatially periodic steady solutions are unstable in time-dependent computations and hence they are not Turing patterns (Fig. 9).

Case II: In the second situation, both subsystems are linearly stable ensured by choosing $\beta>0$. However, the full system becomes unstable when the modified Marangoni number reaches a threshold value. Two different examples are presented in Fig. 7 (denoted IIa) and Fig. 8 (denoted IIb), respectively. Note that in Fig. 7 $\zeta_m=0$ while in Fig. 8 $\xi_m=0$ and hence as we emphasized in Sec. II B, ζ in Fig. 7 and ξ in Fig. 8 do not correspond to true concentrations but rather combinations of concentrations. In case IIa, $M_\zeta<0$ and $M_\xi>0$ while in case IIb, $M_\zeta>0$ and $M_\xi<0$. The dispersion curves exhibit a range of unstable wavenumbers with a real (case IIa) or complex (case IIb) growth rate (onset through a Hopf bifurcation but now $k_{\max,c}\neq 0$ and hence the solution is not uniform in space). The instability is always a finite wavelength instability since as noted previously the coupling does not affect the dispersion curves in the vicinity of $k=0$, i.e., the wavenumbers near $k=0$ are always stable. By increasing the modified Marangoni number even further, a second range of unstable wavenumbers may appear as indicated by the neutral stability curves [Figs. 7(b) and 8(b)].

In the nonlinear regime the behavior of the full system for the different subcases can be understood from time-dependent computations of Eqs. (28). Such computations can also be used to check the linear stability predictions for the behavior of the uniform state $(1,\zeta_0,\xi_0)$ at onset. The numerical scheme is a Crank-Nicholson-type implicit scheme with the x-derivatives approximated by central differences. The time step is chosen dynamically to control several aspects of the simulation. In case I pictured in Fig. 9, the uniform state used as the initial condition is altered by a small sinusoidal perturbation of maximum amplitude 0.1. When $M=0$, the bistable system evolves towards a Turing pattern as expected. When $M\neq 0$, at small times the system evolves into a spatially periodic cellular pattern as expected from the linear stability analysis that predicts a real growth rate. This pattern, however, does not saturate to a Turing pattern as in Fig. 9(a) but rather develops a temporal oscillation in addition to the spatial one, leading to a spatio-temporal breather-like pattern. In case IIa displayed in Fig. 10 the uniform state is disturbed by random noise of maximum amplitude 0.1. Again, as the growth rate is real, for small times the system

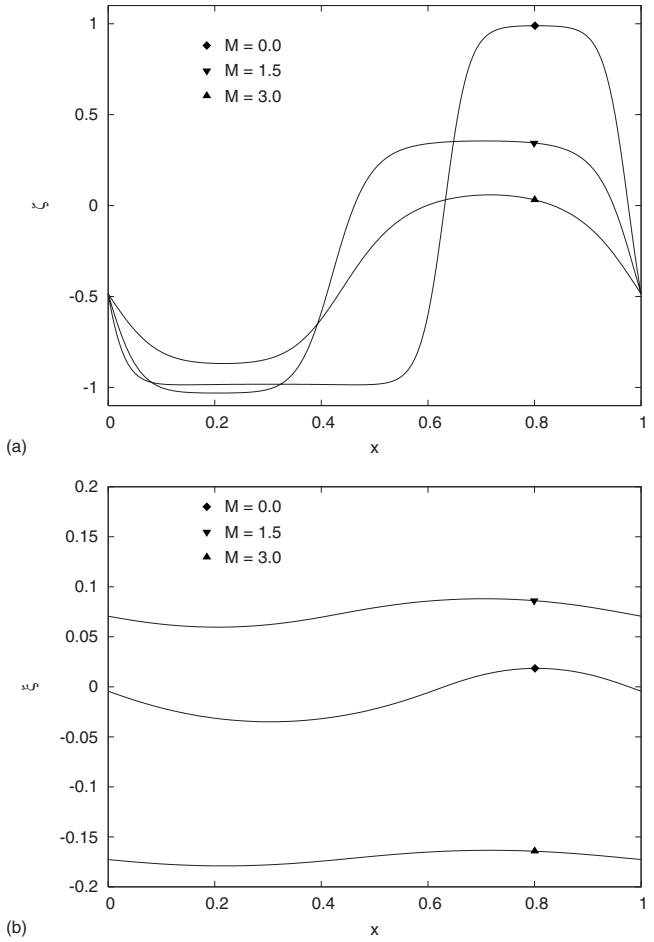

FIG. 6. Case Ib (cf. Fig. 4). Profile of (a) the activator ζ and (b) the inhibitor ξ for parameters as in Fig. 5.

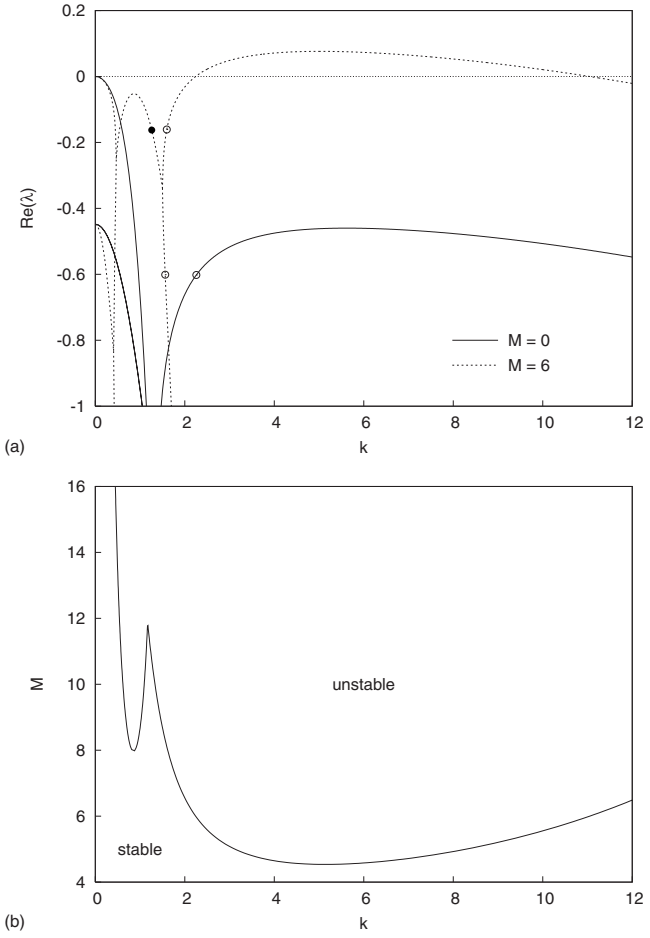

FIG. 7. Case IIa for $\delta=1000$, $K=1$, $\zeta_m=0$, $\xi_m=1$, $a_0=-0.5$, $a_1=0.5$, $B=1$, and $W=1$. (a) Dispersion curves for two different values of the modified Marangoni number: $M=0$ (solid lines) and $M=6$ (dashed lines). For $M=0$ all modes are stable (with the $k=0$ mode being neutrally stable) whereas for $M=6$ a range of unstable modes exists. A circle (◦) or bullet (•) on a curve indicates real or complex growth rates, respectively. (b) Corresponding stability map.

evolves into a spatial pattern that grows monotonically in time without any lateral displacement. For large times both free surface and activator evolve into a number of fronts which continuously collide with each other. These coalescence events are deeply inelastic resulting in annihilation of the colliding fronts. Front solutions will be examined in detail in the next section.

In Fig. 11 for case IIb the initial condition is the same with that in Fig. 10 for case IIa. For small times (not shown) the system evolves into a spatio-temporal oscillation consistent with the linear stability analysis that predicts a complex growth rate with $k_{\max,c}\neq 0$. In fact at about $t=20$ a time dependent spatially periodic pattern appears with a wavelength matching the most unstable wavelength for this configuration [Fig. 8(a)]. Overall the system now evolves much more slowly compared to the situation shown in Fig. 10. Eventually, for large times a temporal oscillation with two frequencies, a small (between two consecutive curves) and a large (every ~200–300 time units) sets in. These are due to the coupling between the two subsystems: time-dependent computations with the pure chemical subsystem, show that when the primary bifurcation is a Hopf bifurcation, in the nonlinear regime a single oscillation is observed.

VI. FRONT- AND PULSE-DRIVEN HYDRODYNAMIC INSTABILITIES

In addition to Turing structures, traveling waves may arise in the excitable/bistable reaction-diffusion subsystem. Through the surface tension gradient such waves may drive a flow in the film, destabilize the flat surface and trigger nonlinear traveling hydrodynamic waves.

We then seek traveling wave solutions of the full system (28) propagating at a constant speed c. We introduce the moving coordinate transformation $z=x-ct$ and we obtain an eight-dimensional dynamical system

$$\left[ch+\frac{1}{3}Bh^3h'-\frac{1}{3}Wh^3h'''+\frac{1}{2}Mh^2\xi'\right]'=0, \tag{37a}$$

$$\left[c\zeta+\frac{1}{2}Bh^2(\zeta_m+\zeta)h'-\frac{1}{2}Wh^2(\zeta_m+\zeta)h'''+Mh(\zeta_m+\zeta)\xi'+\frac{1}{\delta}\zeta'\right]'+K(\zeta-\zeta^3-\xi)=0, \tag{37b}$$

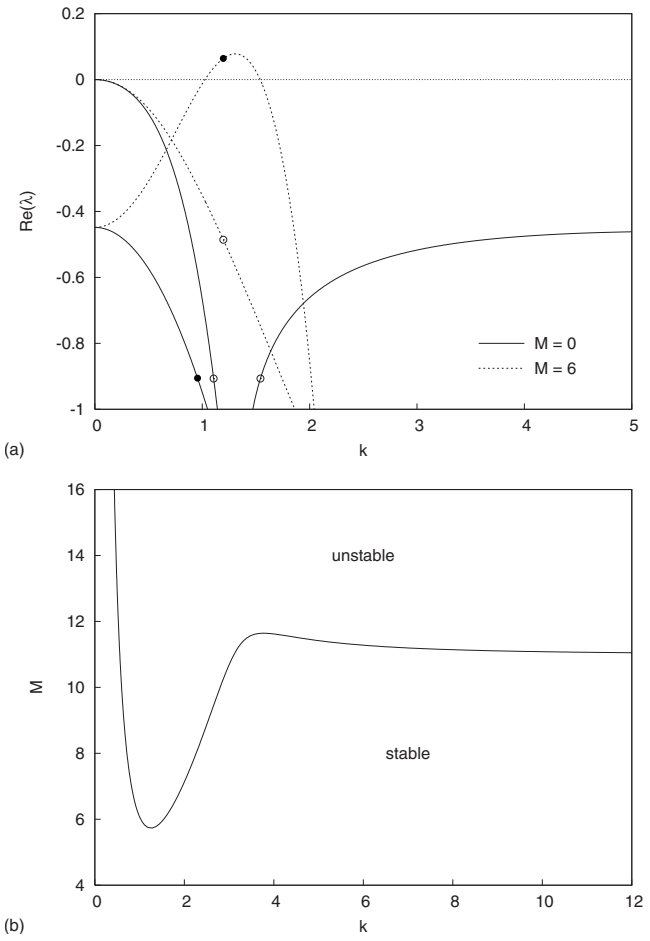

FIG. 8. Case IIb for $\delta=1000$, $K=1$, $\zeta_m=1$, $\xi_m=0$, $a_0=-0.5$, $a_1=0.5$, $B=1$, and $W=1$. (a) Dispersion curves for two different values of the modified Marangoni number: $M=0$ (solid lines) and $M=6$ (dashed lines). For $M=0$ the steady state is linearly stable whereas for $M=6$ it is unstable. A circle (◦) or bullet (•) on a curve indicates real or complex growth rates, respectively. (b) Corresponding stability map.

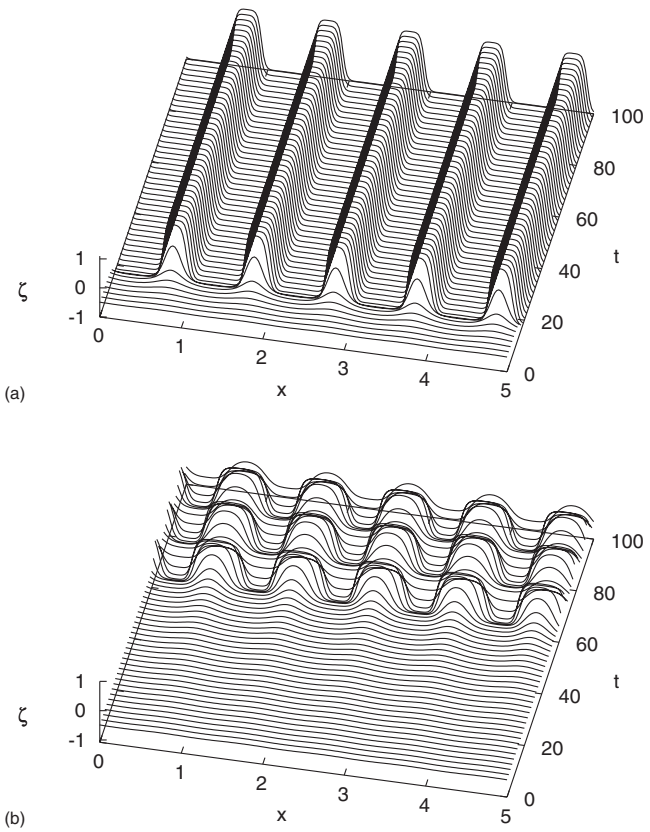

FIG. 9. Case Ib (cf. Fig. 4). Time-dependent computations for modified Marangoni numbers (a) $M=0$ and (b) $M=2$. In both cases the initial condition is a sinusoidal perturbation of amplitude 0.1 superimposed to the uniform state. The domain size is $L=5$ (≃5 times the fastest growing wavelength obtained in the linear stability analysis; see Fig. 4), the number of spatial grid points is 1000, and the time interval between two consecutive profiles is $\Delta t=2$. For $M=0$ the chemical subsystem evolves into a Turing pattern, whereas for $M=2$ a breather-like pattern is found.

$$\left[c\xi+\frac{1}{2}Bh^2(\xi_m+\xi)h'-\frac{1}{2}Wh^2(\xi_m+\xi)h'''+Mh(\xi_m+\xi)\xi'+\xi'\right]'+\zeta-a_1\xi-a_0=0, \tag{37c}$$

where the primes denote differentiation with respect to z. Only solutions that are bounded as $z\to\pm\infty$ are relevant. Equations (37) then define a nonlinear eigenvalue problem for the wave speed c. The traveling wave solutions of Eqs. (28) have a simple description in the phase space associated with Eqs. (37): homogeneous states of Eqs. (28) correspond to fixed points of Eqs. (37) while traveling wave trains, pulses, and fronts correspond to periodic, homoclinic, and heteroclinic orbits, respectively.

Interestingly, some analytical steady solutions of Eqs. (37) can be derived for $M=0$, $a_1>1$, and in the limit $\delta K\ll 1$. Looking for solutions with $c=0$ which are bounded as $z\to\pm\infty$ we have to leading-order

$$h=1, \tag{38a}$$

$$\frac{1}{\delta K}\zeta_{xx}-\zeta^3+\left(1-\frac{1}{a_1}\right)\zeta+\frac{a_0}{a_1}=0, \tag{38b}$$

$$\xi=\frac{\zeta-a_0}{a_1}. \tag{38c}$$

In the front case Hagberg[69] obtained the solution

$$\zeta=-\sqrt{2}a_f\tanh(a_f\sqrt{\delta K}x), \tag{39a}$$

where

$$1-\frac{1}{a_1}=2a_f^2 \quad \text{and} \quad a_0=0. \tag{39b}$$

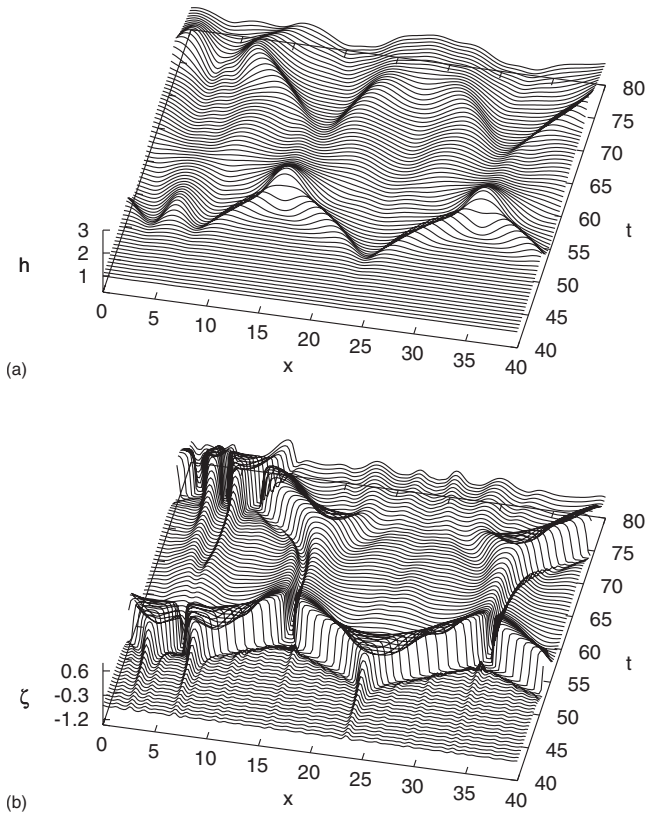

FIG. 10. Case IIa (cf. Fig. 7). Evolution of (a) the free surface and (b) the activator for $M=6$. The uniform state is disturbed by random noise of maximal amplitude 0.1. The domain size is $L=40$ ($\simeq 40$ times the fastest growing wavelength obtained in the linear stability analysis; see Fig. 7), the number of spatial grid points is 1000 and the time interval between two consecutive curves is $\Delta t=8/15$.

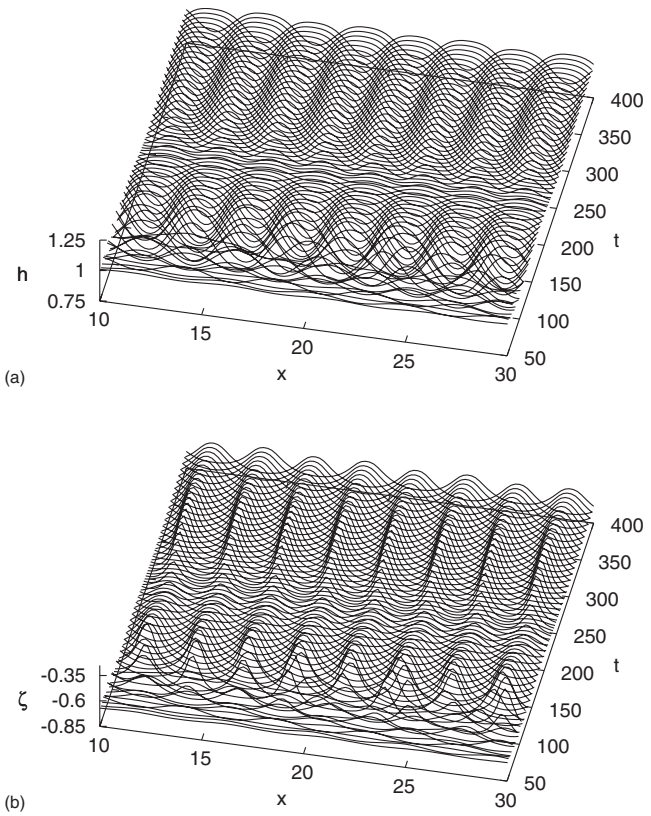

FIG. 11. Case IIb (cf. Fig. 8). Evolution of (a) the free surface and (b) the activator for $M=6$. The initial condition is as in Fig. 10. The domain size is $L=40$ [only the interval (10,30) is displayed], the number of spatial grid points is 1000, and the time interval between two consecutive curves is $\Delta t=4$.

In this limit the front is a hyperbolic tangent. In the pulse case we find

$$\zeta = \frac{a_p\sqrt{1-b_p^2}}{\sqrt{2}}\left(\frac{2}{1+b_p\cosh(a_p\sqrt{\delta K}x)} - \frac{1}{1-b_p^2}\right), \qquad (40a)$$

where a_p and b_p are defined by

$$1-\frac{1}{a_1} = a_p^2\left(\frac{3}{2(1-b_p^2)} - 1\right) \quad \text{and} \quad \frac{a_0}{a_1} = \frac{a_p^3 b_p^2}{\sqrt{2}(1-b_p^2)^{3/2}}. \qquad (40b)$$

In the general case, however, traveling wave solutions can only be obtained numerically. This was done by using the continuation software AUTO97 (Refs. 78–80) (the analytical solutions presented above have also been confirmed numerically). We distinguish two main situations according to the type of wave propagating in the chemical system: *case III*, a front connecting the two concentration states at the far ends of the domain, $(\zeta_\pm, \xi_\pm)$ with $(\zeta_+, \xi_+) > (\zeta_-, \xi_-)$; and *case IV*, a pulse.

Depending on the stability characteristics of the two states in case III we can further distinguish two subcases. Case IIIa, the state with the larger concentrations, (ζ_+^a, ξ_+^a), is the more stable state invading that with the smaller concentrations, (ζ_-^a, ξ_-^a), the less stable one (the more stable state requires a stronger perturbation to destabilize it[69]). Case IIIb, the role of the two states is now reversed: the state with the smaller concentrations, (ζ_-^b, ξ_-^b), is now the more stable state invading that with the larger concentrations, (ζ_+^b, ξ_+^b), the less stable one.

The first subcase is depicted in Fig. 12. The chemical front generates a surface tension gradient on the interface which then induces a solitary wave there. Depending on the sign of the modified Marangoni number, we obtain either a positive-hump wave ($M>0$) or a hollow negative-hump one ($M<0$) in the surface profile. Roughly speaking, as the modified Marangoni number departs from zero, the height of the surface wave becomes larger while the front of the chemical system is increasingly smoothed out.

The second subcase is shown in Fig. 13. The situation is inverted with respect to the free surface: a negative-hump wave propagates on the free surface when $M>0$ and becomes a positive-hump one as M crosses zero. The difference between these two subcases is due to the role played by the surface active species of the bistable system: in case IIIb the inhibitor which acts directly on the surface tension, has its concentration at a high level ahead of the front and at a low level behind it. The direction of the resulting Marangoni flow is then opposite to that of the wave; we shall return to this point shortly. In case IIIa the opposite applies: both wave and Marangoni flow are now in the same direction. In case IV (Fig. 14), a pulse instead of a front propagates in the excitable system and induces either a positive-hump solitary

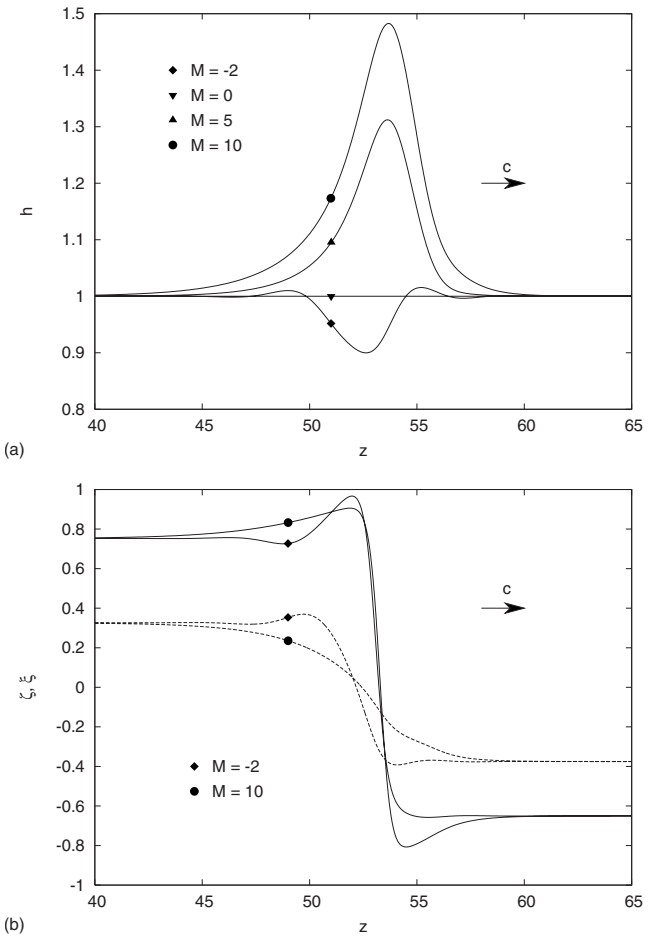

FIG. 12. Case IIIa: The large/small front concentrations are the more stable/less stable states, respectively. $K=10$, $\delta=1$, $\zeta_m=1$, $\xi_m=1$, $a_0=0.1$, $a_1=2.0$, $B=1$, and $W=1$. (a) Free surface h for several values of the modified Marangoni number M between -2 and 10. (b) Corresponding profiles of ζ (solid lines) and ξ (dashed lines).

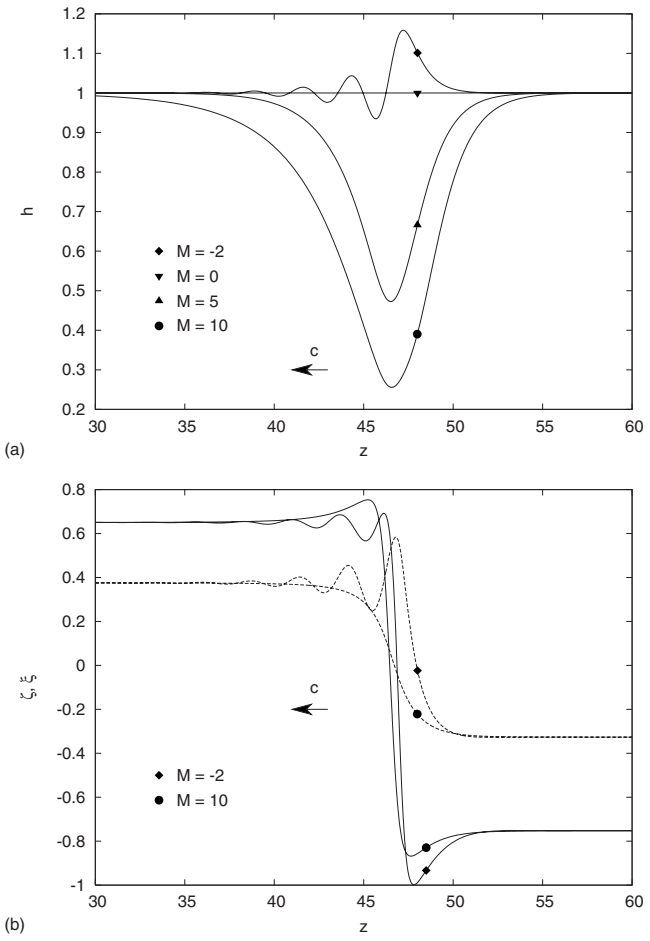

FIG. 13. Case IIIb: The large/small front concentrations are the less stable/more stable states, respectively. $K=10$, $\delta=1$, $\zeta_m=1$, $\xi_m=1$, $a_0=-0.1$, $a_1=2.0$, $B=1$, and $W=1$. (a) Free surface h for several values of the modified Marangoni number M between -2 and 10. (b) Corresponding profiles of ζ (solid lines) and ξ (dashed lines).

pulse ($M>0$) or a negative-hump one ($M<0$) on the free surface. Note that here $\zeta_m=\xi_m=0$ and hence ζ,ξ are not true concentrations but correspond to combinations of concentrations.

Note that $(\zeta_+^a,\xi_+^a)\neq(\zeta_+^b,\xi_+^b)$ and $(\zeta_-^a,\xi_-^a)\neq(\zeta_-^b,\xi_-^b)$ and hence the need to distinguish between two subcases when fronts propagate in the chemical subsystem. In case IV, however, when a pulse propagates in the excitable system, the pulse connects the same state at the two ends of the domain. Hence, for pulses only a single subcase is considered. Note also that due to the reflection symmetry of our system in the streamwise direction, changing the direction of propagation for the pulses in Fig. 14 produces exactly the same pulses and humps for the free surface. The same invariance also exists for the fronts case (both for the pure reaction-diffusion system and the coupled system) due to the reflection symmetry, e.g., in case IIIa depicted in Fig. 12, changing the location of the two states so that (ζ_-^a,ξ_-^a) is now at the left end of the domain and (ζ_+^a,ξ_+^a) at the right end gives the same front and the same hump for the free surface but now propagating from the right to the left.

The dependence of the wave speed on the modified Marangoni number for each situation is depicted in Figs. 15–17, respectively. For cases IIIa and IV the speed is a monotonically increasing function of M and hence the coupling between the two subsystems leads to increasing the speed of the chemical wave for the excitable as well as for the bistable system. For case IIIb, we observe a decrease of $|c|$ ($c<0$ in Fig. 13). This is not surprising as in cases IIIa and IIIb the surface active species ξ has similar profiles implying similar Marangoni flows at the film surface. Specifically, in both cases the Marangoni flow is in the positive direction as is evident from the Marangoni contribution $-M\xi_x h$ to the flow field in Eq. (27). However, because the wave fronts move in opposite directions, the Marangoni flow enforces the propagation of the IIIa fronts and slows down that of IIIb ones.

An exception is found for small values of M in case IIIa as shown in Fig. 15(a) in contrast to case IIIb shown in Fig. 16(a) and although a symmetry between the two types of propagating fronts exists for $M=0$,

$$z\to -z,\quad \hat{c}\to -\hat{c},\quad \hat{h}\to\hat{h},\quad \hat{\zeta}\to -\hat{\zeta},\quad \hat{\xi}\to -\hat{\xi},\quad a_0\to -a_0, \tag{41}$$

where the hats refer to the steady states at $M=0$, e.g., $\hat{c}\equiv c(M=0)$ and $\hat{h}\equiv h(M=0)=1$. The symmetry is evident

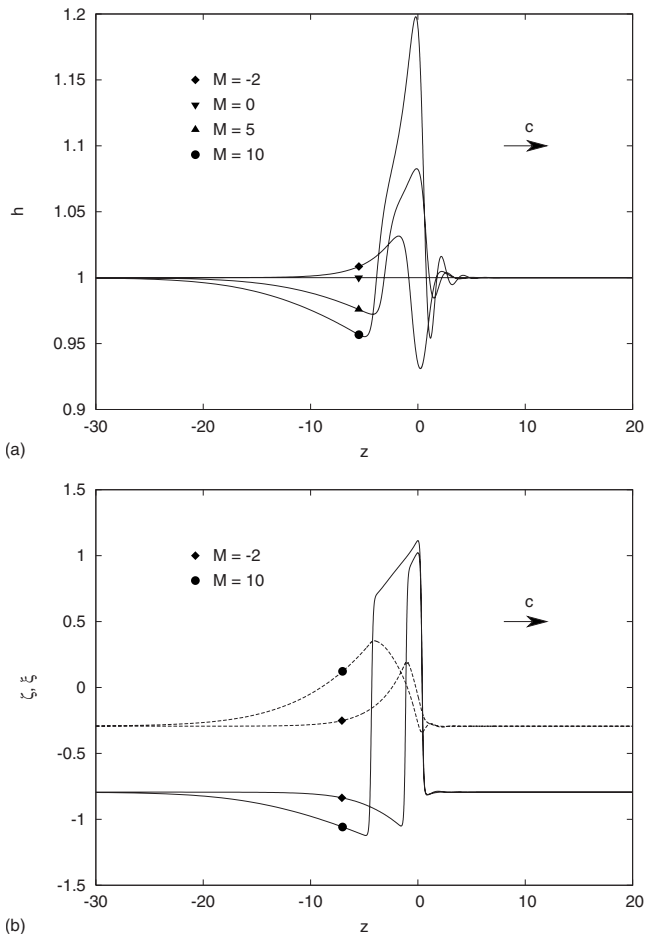

FIG. 14. Case IV: Solitary pulse for the chemical subsystem with $K=100$, $\delta=1$, $\zeta_m=0$, $\xi_m=0$, $a_0=-0.5$, $a_1=1.0$, $B=1$, and $W=1$. (a) Free surface h for several values of the modified Marangoni number M between -2 and 10. (b) Corresponding profiles of ζ (solid lines) and ξ (dashed lines).

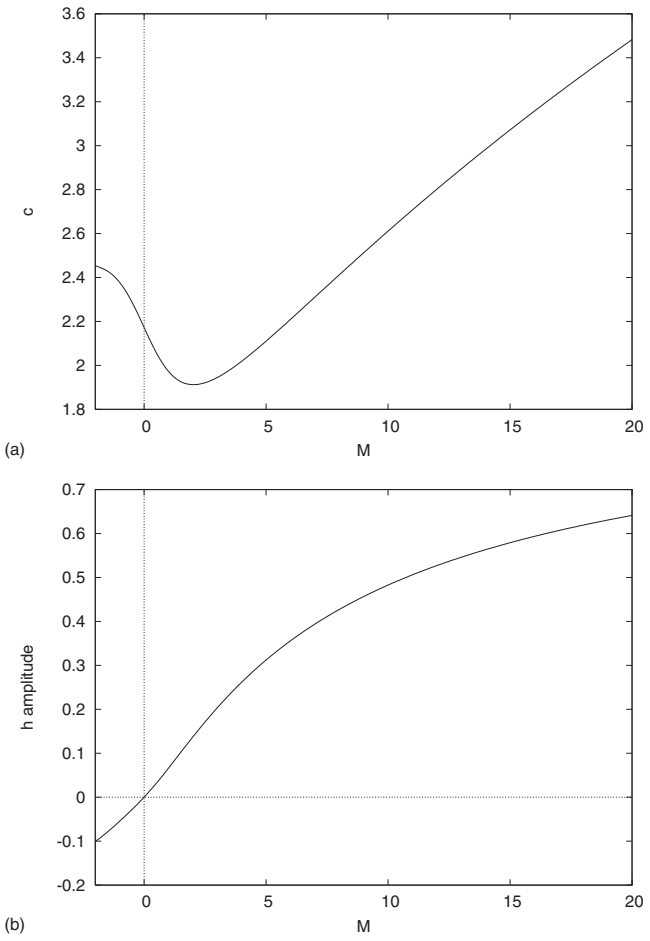

FIG. 15. Case IIIa (cf. Fig. 12). (a) Bifurcation diagram for the speed c as a function of the modified Marangoni number M. (b) Amplitude of the corresponding free-surface wave as a function of M.

from Figs. 15(a) and 16(a), where for $M=0$, $|c|\simeq 2.2$ for both cases. However, this symmetry is broken for small M, unless $\zeta_m=\xi_m=0$. More precisely, if we consider $M\ll 1$ and denote with the subscript 1 the first-order deviations of the variables, e.g., $h=\hat{h}+h_1+O(M^2)$, Eqs. (37) yields at first order in M

$$\left[\hat{c}h_1+\frac{1}{2}Bh_1'-\frac{1}{3}Wh_1'''+\frac{1}{2}M\hat{\xi}'\right]'=0, \tag{42a}$$

$$\left[\hat{c}\zeta_1+c_1\hat{\zeta}+\frac{1}{2}B(\zeta_m+\hat{\zeta})h_1'-\frac{1}{2}W(\zeta_m+\hat{\zeta})h_1'''+M(\zeta_m+\hat{\zeta})\hat{\xi}'+\frac{1}{\delta}\zeta_1'\right]'+K(\zeta_1-3\hat{\zeta}^2\zeta_1-\xi_1)=0, \tag{42b}$$

$$\left[\hat{c}\xi_1+c_1\hat{\xi}+\frac{1}{2}B(\xi_m+\hat{\xi})h_1'-\frac{1}{2}W(\xi_m+\hat{\xi})h_1'''+M(\xi_m+\hat{\xi})\hat{\xi}'+\xi_1'\right]'+\zeta_1-a_1\xi_1=0, \tag{42c}$$

which show that for $\zeta_m=\xi_m=0$ the symmetry exists

$$M\to M,\quad c_1\to c_1,\quad h_1\to -h_1,\quad \zeta_1\to\zeta_1,\quad \xi_1\to\xi_1 \tag{43}$$

between the first-order quantities of the two cases. All signs in Eq. (43) are reversed if $M\to -M$ instead of $M\to M$. A bifurcation diagram illustrating this symmetry is given in Fig. 18, where the speed c of the traveling waves increases monotonically as a function of M as in case IIIb, whichever direction the front travels in. This suggests that the decrease of c with M for small values of M in Fig. 15(a) is connected with nonzero values for ζ_m, ξ_m.

In terms of the amplitude of the free surface deflection, we find that in general this amplitude increases with increasing absolute value of the modified Marangoni number [Figs. 15(b), 16(b), and 17(b)]. This implies that for the chemically driven hydrodynamic system the Marangoni coupling has the opposite effect compared to that of surface active agents on thin films, where in general insoluble surfactants have a stabilizing influence.[37,38] Here it is the instability of the reactive surfactants that drives the deflection of the surface.

The behavior of the wave profiles in the limit $z\to\pm\infty$ can be examined by performing a linear stability analysis of the system (37) around the relevant fixed points. The eigenvalues of the linearized system around the sole fixed point in the pulse case are displayed in Fig. 19 for modified Ma-

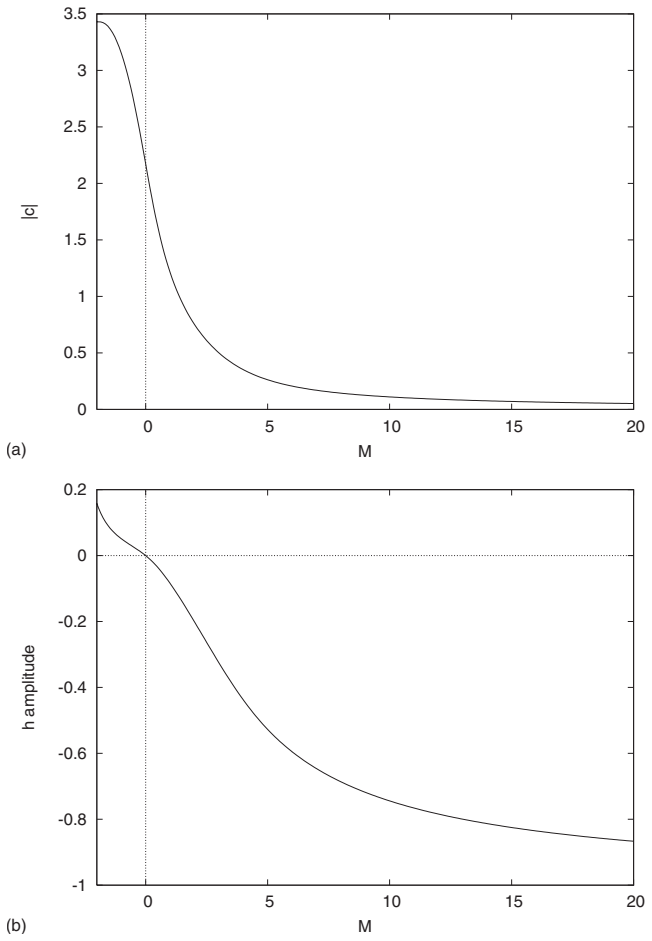

FIG. 16. Case IIIb (cf. Fig. 13). (a) Bifurcation diagram for the absolute value of the speed $|c|$ as a function of the modified Marangoni number M. (b) Amplitude of the corresponding free-surface wave vs M.

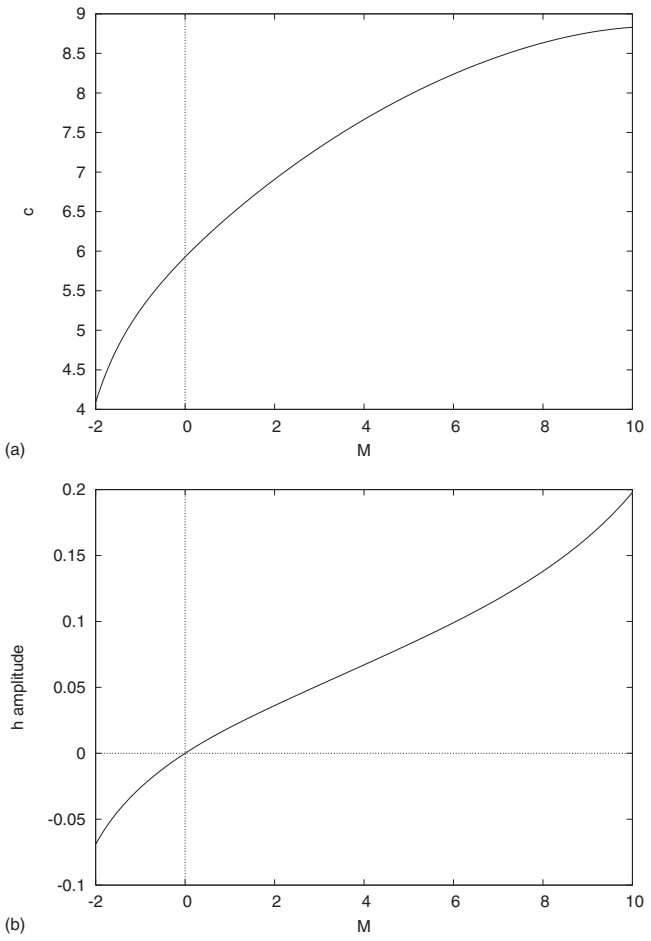

FIG. 17. Case IV (cf. Fig. 14). (a) Bifurcation diagram for the speed c as a function of the modified Marangoni number M. (b) Amplitude of the corresponding free-surface wave vs M.

rangoni numbers ranging from 0 to 10. We note, for instance, that for $M=5$, the wave profiles have an oscillatory behavior for $z\to+\infty$ and an exponential behavior for $z\to-\infty$, since the fixed point in that case has two complex eigenvalues with negative real parts, one zero eigenvalue (which exists for all values of the parameters; a consequence of the translational invariance of the system in the streamwise direction), and three positive real eigenvalues. This is reflected in the corresponding profiles displayed in Fig. 14 and confirmed in Fig. 19. Hence the Marangoni stresses also influence the way the pulse connects to the uniform state.

The existence of a special class of solutions, namely, those which are stationary in a moving frame, raises the question of relevance/stability of these solutions which is related to the way they attract initial conditions. An answer to this question can be given by time-dependent computations of the full system (28). The numerical method was described in Sec. V. In cases IIIa and IIIb, depicted in Figs. 20 and 21, respectively, the initial condition is a Gaussian distribution of amplitude 0.3 and −0.3, respectively, in the middle of the domain added to the homogeneous base state. Due to the reflection symmetry in the streamwise direction, two fronts with opposite speeds appear in the bistable system and induce two solitary waves at the free surface, positive ones in case IIIa and negative ones in case IIIb. The dip in case IIIa (or peak in case IIIb) appearing in the h-profile at the location of the initial perturbation decays slowly and remains visible for a long period of time. These computations indicate the stability of the fronts/pulses for the concentration/free surface. In case IV (Fig. 22), the same kind of initial condition as in cases III is used but with a smaller spatial extension and a larger amplitude of 1.6 to overcome the excitability threshold and to obtain a pulse in the excitable system. After a short transient ($t\sim1$) two counterpropagating pulses appear in the excitable system that move with constant speed [again due to the reflection symmetry, Fig. 22(b)]. On the free surface two solitary waves with opposite speeds arise as well as a depression at the center of the domain which slowly spreads and decays. These computations indicate the stability of the pulse traveling wave solutions in this case.

VII. CONCLUSION

We have presented a model for a horizontal liquid film on a solid substrate whose free surface is covered by two species undergoing an autocatalytic chemical reaction modeled with the well studied FitzHugh-Nagumo equations involving two dynamic variables, the activator and the inhibitor. Depending on the values of the chemical parameters, the

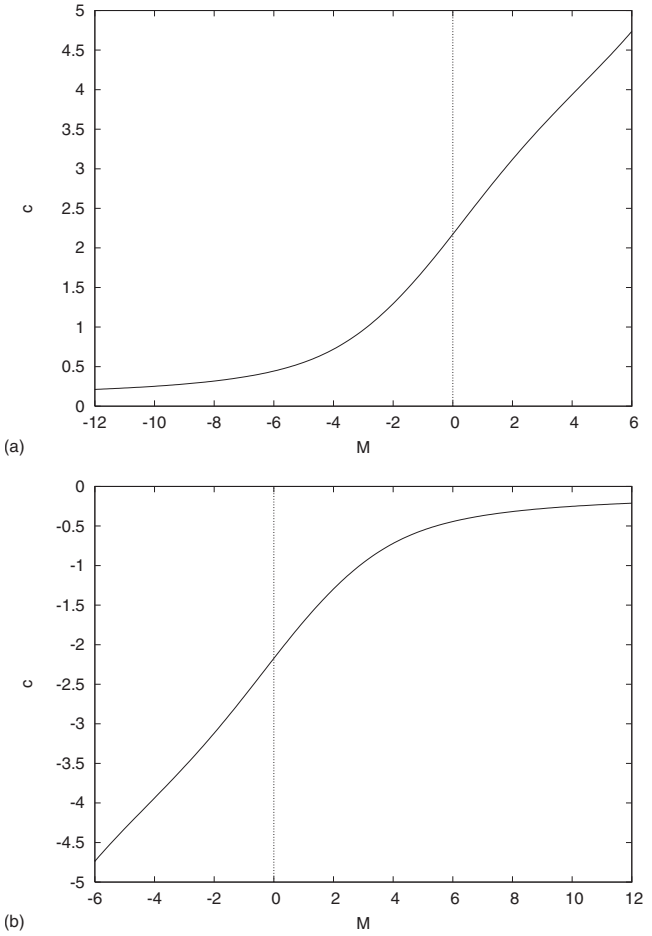

FIG. 18. Bifurcation diagram in the front case for the speed c as a function of M with $\zeta_m=\xi_m=0$. The values of the remaining dimensionless groups for (a) and (b) are given in Figs. 12 and 13, respectively. In contrast to Figs. 15(a) and 16(a), a symmetry exists between (a) and (b).

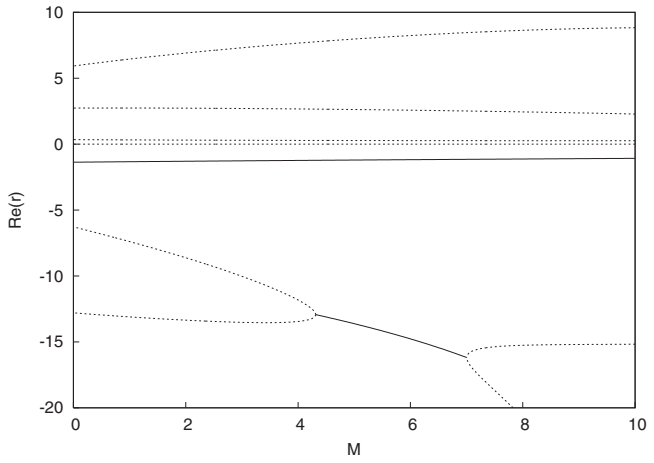

FIG. 19. Eigenvalues r associated with the fixed point corresponding to the base state of the system in case IV (see Fig. 14). The corresponding wave speeds that enter the computation are given in Fig. 17. For a given value of M there are eight eigenvalues. For example, for $M=5$ we obtain four real eigenvalues (denoted by dotted lines), three positive ones and one equal to zero, and two complex pairs (denoted by solid lines) with negative real parts.

chemical subsystem allows for propagating waves, fronts and pulses, corresponding to the bistable and excitable regimes, respectively.

The inhibitor was assumed to possess much stronger surfactant properties than the activator. Hence, gradients in its concentration induce solutal Marangoni stresses along the free surface of the film causing convection below the surface and therefore, as a feedback mechanism, a redistribution of the surfactant at the surface. The coupled Navier-Stokes/reaction-diffusion equations and associated wall/free-surface boundary conditions were simplified using a long-wave approximation resulting in a system of three coupled nonlinear partial differential equations for the evolution in time and space of the free-surface profile and the concentration profiles of the two species. These equations allowed us to carry out a theoretical and numerical analysis of the coupled system.

The steady state consists of a flat film with uniform concentrations of the two species corresponding to those obtained from the nullclines of the pure reaction-diffusion system. A linear stability analysis revealed that the steady state can become unstable in two different ways. In the first case the uniform state of the chemical subsystem in the absence of hydrodynamics is unstable. This instability is either of the Turing-type, resulting in spatially periodic cellular structures, or of the Hopf-type resulting in temporal oscillations. Coupling the two subsystems through the Marangoni effect and increasing M from zero, makes the full system unstable as

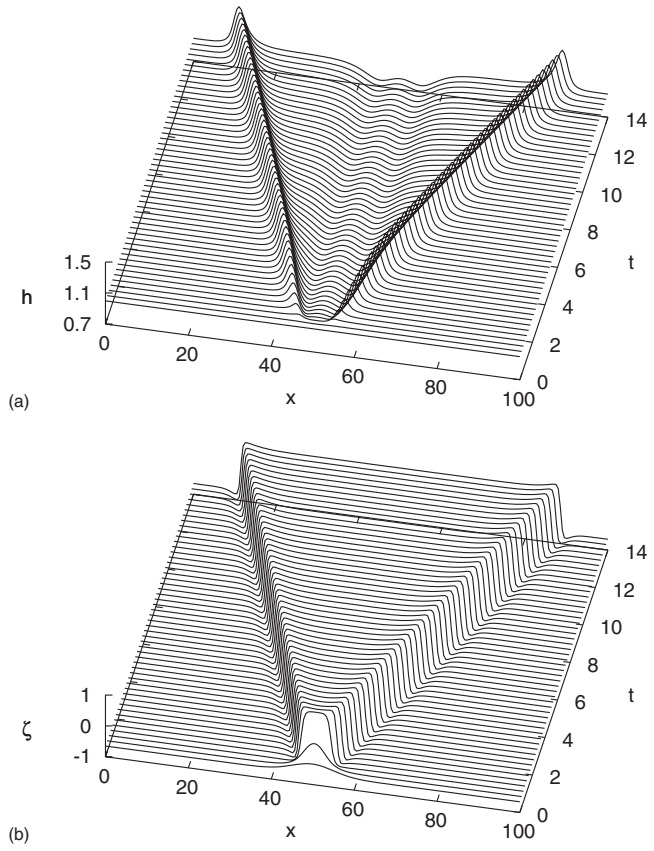

FIG. 20. Case IIIa (see Fig. 12): Time evolution for $M=10$. The domain size is $L=100$, the number of spatial grid points is 1000, and the time interval between two consecutive curves is $\Delta t=0.28$. (a) Free surface: two positive-hump solitary waves with opposite speeds travel along the surface. (b) The activator: two fronts with opposite speeds propagate in the system.

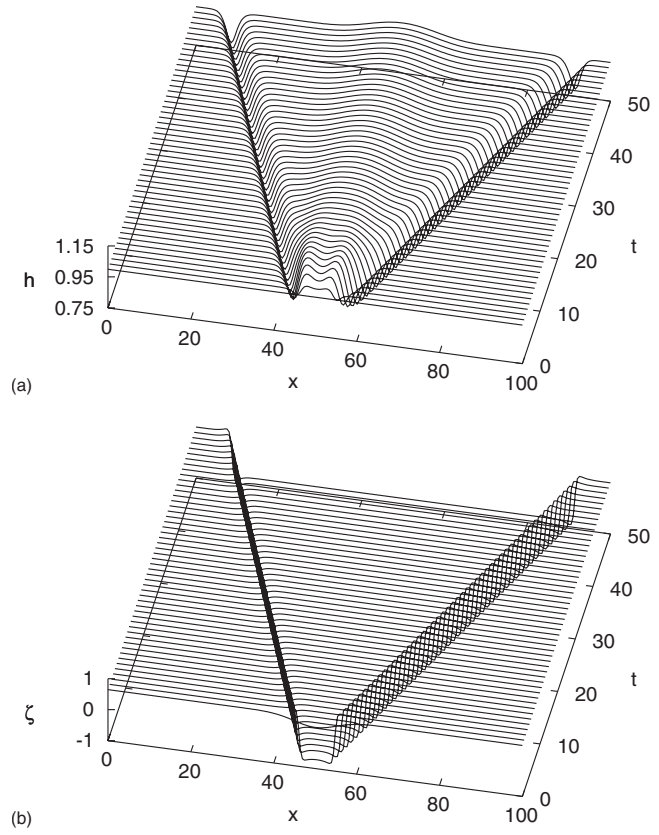

FIG. 21. Case IIIb (see Fig. 13): Time evolution for $M=2$. The domain size is $L=100$, the number of spatial grid points is 1000, and the time interval between two consecutive curves is $\Delta t=1$. (a) Free surface: two negative-hump solitary waves with opposite speeds travel along the surface. (b) The activator: two fronts with opposite speeds propagate in the system.

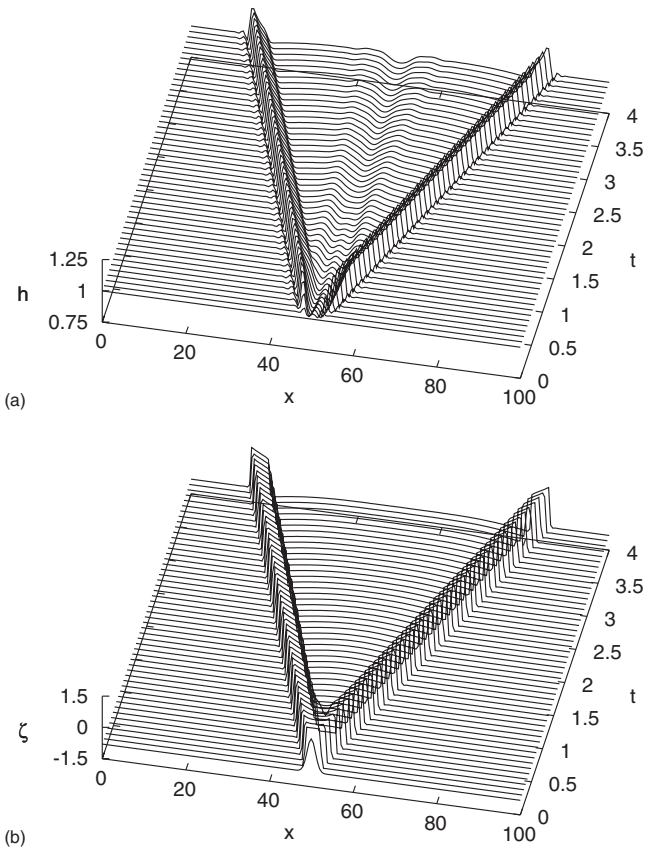

FIG. 22. Case IV (see Fig. 14): Time evolution for $M=10$. The domain size is $L=100$, the number of spatial grid points is 1000, and the time interval between two consecutive curves is $\Delta t=0.08$. (a) Free surface: two solitary waves with opposite speeds travel along the surface. Note the presence of a slowly decaying residual dip due to the initial condition. (b) The activator: the resting pulse formed at the beginning splits into two counterpropagating solitary pulses.

well, i.e., a hydrodynamic instability is now observed. But further increasing M, the Marangoni stresses can stabilize the coupled system and for sufficiently large M can suppress the instabilities all together. The nature of the primary bifurcation can vary from one with real growth rate to one with complex growth rate at onset (Hopf). For the case of real growth rate the coupling between the two subsystems can alter a Turing pattern for the pure chemical subsystem to a breather-like pattern.

In the second case, both subsystems are linearly stable. The coupled system, however, can become unstable because of increased coupling for M above a threshold value. Again the nature of the primary bifurcation changes from one with a real growth rate to one with a complex growth rate (Hopf). In the case of a real growth rate, time-dependent computations reveal that in the nonlinear regime the system evolves into a series of fronts characterized by continuous coalescence events leading to annihilation of colliding fronts. In the Hopf case the system evolves into a spatial pattern that oscillates in time in a complex fashion.

In principle, one can imagine a third case having an unstable base state of the decoupled hydrodynamic subsystem, i.e., the liquid film is itself unstable without any reacting surfactant, like for falling films. The coupling between hydrodynamics and reaction-diffusion process then could also have a stabilizing or destabilizing influence. However, in the present study we did not include a destabilizing influence for the decoupled liquid film. Similarly, systems of increased degree of complexity can be set up by coupling reaction-diffusion processes with other instabilities such as the long-wave thermocapillary Marangoni instability for horizontal films[81,82] and falling films[30,32] or the spinodal dewetting instability for ultrathin films.[83–85]

Further, we examined the existence of traveling waves on the free surface driven by solitary pulses and fronts in the respective excitable and bistable systems. In the former case, we demonstrated the existence of solitary pulses on the free surface. In the latter case, chemical fronts were shown to induce a traveling elevation or depression of the free surface. These deformations correspond to positive- and negative-hump solitary pulses, respectively (for $M>0$). In general, for sufficiently strong coupling (large M) between the two subsystems the deformation amplitude increases with the absolute value of M while the absolute value of the propagation speed is an increasing function of M when the wave and Marangoni flow have the same direction and a decreasing one otherwise. [For small coupling (small M), however, the propagation speed may also decrease.] Traveling pulses in the excitable case have been shown to behave in a similar way.

Finally, it is important to emphasize that in the present study we focused on the basic dynamic characteristic of the coupling between the thin film and the reaction-diffusion process, i.e., the influence of the coupling strength through M, while keeping all other parameters constant. However, because of the large number of dimensionless groups involved, we expect other interesting features due to the influence of the purely hydrodynamic or chemical parameters, e.g., a_0 or K. In fact, both uniform state and traveling waves of the chemical subsystem undergo a wide variety of bifurcations when the chemical parameters are varied. Here, it has already been shown that the mean concentrations of activator and inhibitor can significantly alter the bifurcation diagrams [cf. Figs. 15(a) and 18(a)]. The present study may also be altered by considering the activator rather than the inhibitor acting as a surfactant or when both species possess surface active properties.

ACKNOWLEDGMENTS

We acknowledge financial support from the Engineering and Physical Sciences Research Council of the UK (EPSRC) through Grant Nos. GR/S7912 and GR/S01023. S.K. acknowledges financial support from the EPSRC through an Advanced Fellowship, Grant No. GR/S49520. U.T. acknowledges support by the European Union and Deutsche Forschungsgemeinschaft through Grant Nos. MRTN-CT-2004-005728 and SFB 486 B13, respectively.

[1] A. Oron, S. H. Davis, and S. G. Bankoff, "Long-scale evolution of thin liquid films," Rev. Mod. Phys. **69**, 931 (1997).
[2] *Thin Films of Soft Matter*, edited by S. Kalliadasis and U. Thiele (Springer-Wien, New York, 2007).
[3] A. Sharma and R. Khanna, "Pattern formation in unstable thin liquid films," Phys. Rev. Lett. **81**, 3463 (1998).
[4] A. Oron, "Three-dimensional nonlinear dynamics of thin liquid films," Phys. Rev. Lett. **85**, 2108 (2000).
[5] M. Bestehorn and K. Neuffer, "Surface patterns of laterally extended thin liquid films in three dimensions," Phys. Rev. Lett. **87**, 046101 (2001).
[6] U. Thiele, M. G. Velarde, K. Neuffer, and Y. Pomeau, "Film rupture in the diffuse interface model coupled to hydrodynamics," Phys. Rev. E **64**, 031602 (2001).
[7] H.-C. Chang, "Wave evolution on a falling film," Annu. Rev. Fluid Mech. **26**, 103 (1994).
[8] B. Ramaswamy, S. Chippada, and S. W. Joo, "A full-scale numerical study of interfacial instabilities in thin-film flows," J. Fluid Mech. **325**, 163 (1996).
[9] C. Ruyer-Quil and P. Manneville, "Further accuracy and convergence results on the modeling of flows down inclined planes by weighted-residual approximations," Phys. Fluids **14**, 170 (2002).
[10] B. Scheid, C. Ruyer-Quil, U. Thiele, O. A. Kabov, J. C. Legros, and P. Colinet, "Validity domain of the Benney equation including Marangoni effect for closed and open flows," J. Fluid Mech. **527**, 303 (2005).
[11] S. M. Troian, E. Herbolzheimer, S. Safran, and J. Joanny, "Fingering instabilities of driven spreading films," Europhys. Lett. **10**, 25 (1989).
[12] M. Spaid and G. M. Homsy, "Stability of Newtonian and viscoelastic dynamic contact lines," Phys. Fluids **8**, 460 (1996).
[13] J. A. Diez and L. Kondic, "Contact line instabilities of thin liquid films," Phys. Rev. Lett. **86**, 632 (2001).
[14] L. Kondic and J. A. Diez, "On nontrivial traveling waves in thin film flows including contact lines," Physica D **209**, 135 (2005).
[15] K. Kargupta, R. Konnur, and A. Sharma, "Spontaneous dewetting and ordered patterns in evaporating thin liquid films on homogeneous and heterogeneous substrates," Langmuir **17**, 1294 (2001).
[16] V. M. Ha and C. L. Lai, "The onset of stationary Marangoni instability of an evaporating droplet," Proc. R. Soc. London, Ser. A **457**, 885 (2001).
[17] L. W. Schwartz, R. V. Roy, R. R. Eley, and S. Petrash, "Dewetting patterns in a drying liquid film," J. Colloid Interface Sci. **214**, 363 (2001).
[18] L. Mahadevan and Y. Pomeau, "Rolling droplets," Phys. Fluids **11**, 2449 (1999).
[19] U. Thiele, M. G. Velarde, K. Neuffer, M. Bestehorn, and Y. Pomeau, "Sliding drops in the diffuse interface model coupled to hydrodynamics," Phys. Rev. E **64**, 061601 (2001).
[20] P. L. Kapitza, "Wave flow of thin layers of a viscous fluid," Zh. Eksp. Teor. Fiz. **18**, 3 (1948).
[21] P. L. Kapitza and S. P. Kapitza, "Wave flow of thin layers of a viscous fluid: III. Experimental study of undulatory flow conditions," Zh. Eksp. Teor. Fiz. **19**, 105 (1949).
[22] H.-C. Chang and E. A. Demekhin, *Complex Wave Dynamics on Thin Films* (Elsevier, Amsterdam, 2002).
[23] D. J. Benney, "Long waves on liquid films," J. Math. Phys. (Cambridge, Mass.) **45**, 150 (1966).
[24] P.-G. de Gennes, "Wetting: Statistics and dynamics," Rev. Mod. Phys. **57**, 827 (1985).
[25] L. M. Hocking, "The spreading of drops with intermolecular forces," Phys. Fluids **6**, 3224 (1994).
[26] L. M. Pismen and U. Thiele, "Asymptotic theory for a moving droplet driven by a wettability gradient," Phys. Fluids **18**, 042104 (2006).
[27] J. R. A. Pearson, "On convection cells induced by surface tension," J. Fluid Mech. **4**, 489 (1958).
[28] L. E. Scriven and C. V. Sternling, "On cellular convection driven by surface-tension gradients: Effects of mean surface tension and surface viscosity," J. Fluid Mech. **19**, 321 (1964).
[29] D. A. Goussis and R. E. Kelly, "Surface wave and thermocapillary instabilities in a liquid film flow," J. Fluid Mech. **223**, 25 (1991).
[30] S. Kalliadasis, E. A. Demekhin, C. Ruyer-Quil, and M. G. Velarde, "Thermocapillary instability and wave formation on a film falling down a uniformly heated plane," J. Fluid Mech. **492**, 303 (2003).
[31] P. M. J. Trevelyan and S. Kalliadasis, "Wave dynamics on a thin liquid film falling down a heated wall," J. Eng. Math. **50**, 177 (2004).
[32] C. Ruyer-Quil, B. Scheid, S. Kalliadasis, M. Velarde, and R. K. Zeytounian, "Thermocapillary long waves in a liquid film flow. I. Low-dimensional formulation," J. Fluid Mech. **538**, 199 (2005).
[33] B. Scheid, C. Ruyer-Quil, S. Kalliadasis, M. G. Velarde, and R. K. Zeytounian, "Thermocapillary long waves in a liquid film flow. II. Linear stability and nonlinear waves," J. Fluid Mech. **538**, 233 (2005).
[34] C. V. Sternling and L. E. Scriven, "Interfacial turbulence: Hydrodynamic instability and the Marangoni effect," AIChE J. **5**, 514 (1959).
[35] W. Ji and F. Setterwall, "On the instabilities of vertical falling liquid films in the presence of surface-active solute," J. Fluid Mech. **278**, 297 (1994).
[36] V. Y. Shkadov, M. G. Velarde, and V. P. Shkadova, "Falling films and the Marangoni effect," Phys. Rev. E **69**, 056310 (2004).
[37] E. Ruckenstein and R. K. Jain, "Spontaneous rupture of thin liquid films," J. Chem. Soc., Faraday Trans. 2 **70**, 132 (1974).
[38] O. E. Jensen and J. B. Grotberg, "Insoluble surfactant spreading on a thin viscous film: Shock evolution and film rupture," J. Fluid Mech. **240**, 259 (1992).
[39] O. K. Matar, "Nonlinear evolution of thin free viscous films in the presence of soluble surfactant," Phys. Fluids **14**, 4216 (2002).
[40] K. A. Cliffe, S. J. Tavener, and H. Wilke, "Convective effects on a propagating reaction front," Phys. Fluids **10**, 730 (1998).
[41] T. Sakurai, H. Miike, E. Yokoyama, and S. C. Müller, "Initiation front and annihilation center of convection waves developing in spiral structures of the Belousov-Zhabotinsky reaction," J. Phys. Soc. Jpn. **66**, 518 (1997).
[42] O. Inomoto, K. Abe, T. Amemiya, T. Yamaguchi, and S. Kai, "Bromomalonic-acid-induced transition from trigger wave to big wave in the Belousov-Zhabotinsky reaction," Phys. Rev. E **61**, 5326 (2000).
[43] H. Kitahata, R. Aihara, N. Magome, and K. Yoshikawa, "Convective and periodic motion driven by a chemical wave," J. Chem. Phys. **116**, 5666 (2002).
[44] J. J. Tyson, *A Quantitative Account of Oscillations, Bistability and Traveling Waves in the Belousov-Zhabotinskii Reaction: Oscillations and Traveling Waves in Chemical Systems*, edited by R. J. Field and M. Burger (Wiley, New York, 1985).
[45] A. Rovinsky and M. Menzinger, "Interaction of Turing and Hopf bifurcations in chemical systems," Phys. Rev. A **46**, 6315 (1992).
[46] S. K. Scott, *Chemical Chaos* (Clarendon, Oxford, 1993).
[47] E. Meron, "Pattern formation in excitable media," Phys. Rep. **218**, 1 (1992).

[48]R. Goldstein, D. Muraki, and D. Petrich, "Interface proliferation and the growth of labyrinths in a reaction-diffusion system," Phys. Rev. E **53**, 3933 (1996).
[49]C. Elphick, A. Hagberg, B. Malomed, and E. Meron, "On the origin of traveling pulses in bistable systems," Phys. Lett. A **230**, 33 (1997).
[50]S. Tobias and E. Knobloch, "Breakup of spiral waves into chemical turbulence," Phys. Rev. Lett. **80**, 4811 (1998).
[51]M. Bär, A. Hagberg, E. Meron, and U. Thiele, "Front propagation and pattern formation in anisotropic bistable media," Phys. Rev. E **62**, 366 (2000).
[52]K. Eckert and A. Grahn, "Plume and finger regimes driven by an exothermic interfacial reaction," Phys. Rev. Lett. **82**, 4436 (1999).
[53]A. De Wit and G. M. Homsy, "Viscous fingering in reaction-diffusion systems," J. Chem. Phys. **110**, 8663 (1999).
[54]T. Bánsági, D. Horváth, A. Tóth, S. Kalliadasis, and A. De Wit, "Density fingering of an exothermic autocatalytic reaction," Phys. Rev. E **68**, 055301 (2003).
[55]S. Kalliadasis, J. Yang, and A. De Wit, "Fingering instabilities of exothermic reaction-diffusion fronts in porous media," Phys. Fluids **16**, 1395 (2004).
[56]J. D'Hernoncourt, S. Kalliadasis, and A. De Wit, "Fingering of exothermic reaction-diffusion fronts in Hele-Shaw cells with conducting walls," J. Chem. Phys. **123**, 234503 (2005).
[57]P. M. J. Trevelyan, S. Kalliadasis, J. H. Merkin, and S. K. Scott, "Dynamics of a vertically falling films in the presence of a first-order chemical reaction," Phys. Fluids **14**, 2402 (2002).
[58]P. M. J. Trevelyan and S. Kalliadasis, "Dynamics of a reactive falling film at large Péclet numbers. I. Long-wave approximation," Phys. Fluids **16**, 3191 (2004).
[59]P. M. J. Trevelyan and S. Kalliadasis, "Dynamics of a reactive falling film at large Péclet numbers. II. Nonlinear waves far from criticality: Integral-boundary-layer approximation," Phys. Fluids **16**, 3209 (2004).
[60]F. D. Dos Santos and T. Ondarçuhu, "Free-running droplets," Phys. Rev. Lett. **75**, 2972 (1995).
[61]S.-W. Lee and P. E. Laibinis, "Directed movement of liquids on patterned surfaces using noncovalent molecular adsorption," J. Am. Chem. Soc. **122**, 5395 (2000).
[62]Y. Sumino, N. Magome, T. Hamada, and K. Yoshikawa, "Self-running droplet: Emergence of regular motion from nonequilibrium noise," Phys. Rev. Lett. **94**, 068301 (2005).
[63]F. Brochard-Wyart and P.-G. de Gennes, "Spontaneous motion of a reactive droplet," C. R. Acad. Sci., Ser. IIa: Sci. Terre Planetes **321**, 285 (1995).
[64]U. Thiele, K. John, and M. Bär, "Dynamical model for chemically driven running droplets," Phys. Rev. Lett. **93**, 027802 (2004).
[65]K. John, M. Bär, and U. Thiele, "Self-propelled running droplets on solid substrates driven by chemical reactions," Eur. Phys. J. E **18**, 183 (2005).
[66]L. M. Pismen, "Composition and flow patterns due to Chemo-Marangoni instability in liquid films," J. Colloid Interface Sci. **102**, 237 (1984).
[67]Z. Dagan and L. M. Pismen, "Marangoni waves induced by a multistable chemical reaction on thin liquid films," J. Colloid Interface Sci. **99**, 215 (1984).
[68]Y. Q. Buyevich, L. M. Rabinovich, and A. V. Vyazmin, "Chemo-Marangoni convection. I. Linear analysis and criteria of instability," J. Colloid Interface Sci. **157**, 202 (1993).
[69]A. A. Hagberg, "Fronts and patterns in reaction-diffusion equations," Ph.D. thesis, University of Arizona (1994).
[70]H. A. Stone, "A simple derivation of the time-dependent convective-diffusion equation for surfactant transport along a deforming interface," Phys. Fluids A **2**, 111 (1990).
[71]H. Wong, D. Rumschitzki, and C. Maldarelli, "On the surfactant mass balance at a deforming fluid interface," Phys. Fluids **8**, 3203 (1996).
[72]P. Cermelli, E. Fried, and M. E. Gurtin, "Transport relations for surface integrals arising in the formulation of balance laws for evolving fluid interfaces," J. Fluid Mech. **544**, 339 (2005).
[73]G. K. Batchelor, *An Introduction to Fluid Dynamics* (Cambridge University Press, Cambridge, 1967).
[74]S. W. Joo, S. H. Davis, and S. G. Bankoff, "Long-wave instabilities of heated falling films: Two-dimensional theory of uniform layers," J. Fluid Mech. **230**, 117 (1991).
[75]R. V. Birikh, V. A. Briskman, M. G. Velarde, and J. C. Legros, *Liquid Interfacial Phenomena—Oscillations and Instability* (Marcel Dekker, New York, 2003).
[76]A. M. Turing, "The chemical basis of morphogenesis," Philos. Trans. R. Soc. London, Ser. B **237**, 37 (1952).
[77]P. Huerre and M. Rossi, *Hydrodynamic Instabilities in Open Flows: Hydrodynamics and Nonlinear Instabilities*, edited by C. Godrèche and P. Manneville (Cambridge University Press, Cambridge, 1998).
[78]E. Doedel, A. Champneys, T. Fairfrieve, Y. Kuznetsov, B. Sandstede, and X. Wang, "AUTO97: Continuation and bifurcation software for ordinary differential equations," Concordia University, Montreal (available by FTP from ftp.cs.canada.ca in directory pub/doedel/auto) (1997).
[79]E. Doedel, H. B. Keller, and J. P. Kernevez, "Numerical analysis and control of bifurcation problems (I) Bifurcation in finite dimensions," Int. J. Bifurcation Chaos Appl. Sci. Eng. **1**, 493 (1991).
[80]E. Doedel, H. B. Keller, and J. P. Kernevez, "Numerical analysis and control of bifurcation problems (I) Bifurcation in infinite dimensions," Int. J. Bifurcation Chaos Appl. Sci. Eng. **1**, 745 (1991).
[81]A. Oron and P. Rosenau, "On a nonlinear thermocapillary effect in thin liquid layers," J. Fluid Mech. **273**, 361 (1994).
[82]U. Thiele and E. Knobloch, "Thin liquid films on a slightly inclined heated plate," Physica D **190**, 213 (2004).
[83]V. S. Mitlin, "Dewetting of solid surface: Analogy with spinodal decomposition," J. Colloid Interface Sci. **156**, 491 (1993).
[84]A. Sharma, "Relationship of thin film stability and morphology to macroscopic parameters of wetting in the apolar and polar systems," Langmuir **9**, 861 (1993).
[85]U. Thiele, M. G. Velarde, and K. Neuffer, "Dewetting: Film rupture by nucleation in the spinodal regime," Phys. Rev. Lett. **87**, 016104 (2001).